Robust RIS-Assisted MIMO Communication-Radar Coexistence: Joint Beamforming and Waveform Design

Mohamed Rihan, *Senior Member, IEEE*, Alessio Zappone, *Senior Member, IEEE*, and Stefano Buzzi, *Senior Member, IEEE*

***Abstract*— This paper addresses the problem of co-existence between a radar and a communication system that share the same frequency band. In particular, we investigate the role of a reconfigurable intelligent surface (RIS) in improving the performance of both systems and facilitating their co-existence. We consider the optimization problem of maximizing the radar signal to interference plus noise ratio (SINR) with respect to the active transmit beamformer at the radar, the passive RIS reflection coefficients, and the transmit covariance matrices of the communication system, subject to communication outage as well as radar and communication power constraints. This problem is solved through an alternating maximization procedure, first in the ideal scenario of perfect channel state information (CSI), and then in the case of incomplete CSI, using a statistical model of the CSI uncertainty. Numerical results demonstrate the effectiveness of our approach and quantify the beneficial effect of an RIS on the co-existence of a radar and a communication system.**

***Index Terms*— MIMO radar, MU-MIMO, reconfigurable intelligent surface (RIS), coexistence, joint optimization, detection probability, bounded error model, statistical error model.**

I. Introduction

THE explosive growth of bandwidth hungry connection-oriented applications has led to an increasing demand for communication networks with high-speed access capabilities. In 5G and beyond networks, this high-speed access can be provided through exploiting higher frequency bands in the millimeter wave range, also by sharing the spectrum with different radio-based services such as a radar system [1]. Indeed, motivated by the need to increase available spectrum utilization, the topic of co-existence in the same frequency range of radar and communication services has attracted a huge interest in the recent past. At the beginning, the convergence between wireless communications and radar sensing research communities was aiming to share the relatively vacant radar bands with bandwidth hungry communication services. In recent times, instead, the convergence moved to much higher levels of cooperation and integration between the communication and radar sensing systems and services. Such cooperation and integration may be relevant in many applications, like, for instance, enhanced localization and tracking, human activity recognition, connected and automated mobility services, sensing-aided communications, and smart manufacturing [2].

Spectrum sharing between communication and radar systems has been extensively studied over the last two decades to circumvent the spectrum scarcity problem [1], [2], [3], [4], [5], [6]. Allowing the communication and radar systems to share the same spectrum bands produces mutual electromagnetic interference that may degrade the performance of the two systems [3], [4]: in particular the radar transmit power may be large enough to significantly degrade the communication system performance. Several works have introduced many approaches to enable spectrum sharing and optimized coexistence between communication and radar systems such as interference mitigation, spatial separation and beamforming, and waveform design [5]. Most of the proposed coexistence designs concentrate on jointly designing the system transceivers while assuming full knowledge of the channel state information (CSI) of different links involving both the communication and radar systems [6]. Some works increase the degrees-of-freedom (DoFs) of the coexistence design problem by deploying one or more reconfigurable intelligent surfaces (RIS) [7] to re-configure the wireless channels in such a way that enhances the design criteria of the coexistence problem [8], [9], [10]. These surfaces, in their passive version, that we consider here, are made of many metamaterial-based sub-wavelength sized planar elements that have the capability to reflect the incoming signal with a tunable phase shift. By properly controlling the tunable phase shifts of the many reflected waves, the response of the wireless

Manuscript received 1 March 2023; revised 27 June 2023; accepted 10 July 2023. Date of publication 26 July 2023; date of current version 20 November 2023. This work was supported by H2020 Marie Skłodowska-Curie Actions (MSCA) Individual Fellowships (IF) RASECOL, Grant agreement 898354. The associate editor coordinating the review of this article and approving it for publication was D. W. K. Ng. *(Corresponding author: Stefano Buzzi.)*

Mohamed Rihan is with the Department of Electrical and Information Engineering (DIEI), University of Cassino and Southern Lazio, 03043 Cassino, Italy, on leave from the Faculty of Electronic Engineering, Menoufia University, Al Menoufia 6052040, Egypt (e-mail: mohamed.elmelegy@el-eng.menofia.edu.eg).

Alessio Zappone is with the Department of Electrical and Information Engineering (DIEI), University of Cassino and Southern Lazio, 03043 Cassino, Italy (e-mail: alessio.zappone@unicas.it).

Stefano Buzzi is with the Department of Electrical and Information Engineering (DIEI), University of Cassino and Southern Lazio, 03043 Cassino, Italy, and also with the Dipartimento di Elettronica, Informazione e Bioingegneria (DEIB), Politecnico di Milano, 20133 Milan, Italy (e-mail: buzzi@unicas.it).

Color versions of one or more figures in this article are available at https://doi.org/10.1109/TCOMM.2023.3298983.

Digital Object Identifier 10.1109/TCOMM.2023.3298983

channel can be partially controlled, in order to improve the system performance [11], [12], [13]. In particular, RISs permit to extend the network coverage by circumventing blocking obstacles, and to help to concentrate the useful signal where it is needed, thus reducing interference. RISs were originally introduced to enhance the performance of wireless communication systems. Very soon, however, researchers realized their potential in improving the performance of stand-alone radar systems [14], [15], and also of integrated radar and communication systems [16].

A. Related Work

Recently, the null-space projection [3], [4], joint beamforming design [5], [6], spectrum/energy allocation [17], and interference mitigation techniques [18], [19] have been widely investigated for enabling coexistence between radar and communication systems. The use of RIS has shown a great potential to play a significant role in the future of wireless communications by improving signal quality [20], increasing spectral efficiency and reducing energy consumption [21], [24], and providing greater flexibility in the design of wireless communication systems [12]. However, only few works have introduced RIS-aided communication-radar coexistence designs [8], [9], [10]. Paper [8] addresses the spectrum sharing problem between a MIMO radar and a multi-user MISO communication system, where the RIS is used to mitigate the interference generated by the communication BS on the radar system. Specifically, the coexistence design maximized the radar detection probability by jointly optimizing the BS transmit beamformer and the RIS reflection matrix, under BS power budget constraint and communication users' quality of service constraints. The authors of [9] concentrate on studying interference mitigation in dual function radar communication (DFRC) systems. Specifically, they investigated joint waveform design and passive beamforming in RIS-assisted DFRC, through minimizing the multi-user communication interference under strict beampattern constraints to jointly optimize the DFRC waveform and the RIS phase shift reflection matrix. An alternating algorithm based on manifold optimization is here employed to solve the design problem. Differently from the above designs, paper [10] investigated a double-RIS assisted communication radar coexistence scenario to further mitigate the mutual interference by efficient joint beamforming design. The papers [22] and [23] are among the recent works that employed RIS to improve the ISAC system performance for localization and data transmission. The authors of [22] introduced a multi-user ISAC framework, where the RIS assists uplink data transmission and conducts multi-user localization simultaneously. The paper proposes an ISAC transmission protocol, a multi-user location sensing algorithm, and two beamforming algorithms, which can work with discrete RIS phase shifts and require no channel state information (CSI) acquisition. On the other hand, [23] establishes a detailed working process of the proposed RIS-based ISAC system, including the transmission protocol, location sensing, and beamforming optimization.

It is worth mentioning that all the above discussed designs are not robust against CSI errors. Inspired by this, in this paper we seek to investigate robust RIS-aided radar-communication coexistence design while considering statistical CSI error models. Indeed, although ISAC systems can provide high-efficient sensing and communication with the same hardware, mechanisms that enable communication and radar systems to coexist in the same frequency band without interfering with each other are similarly of great interest at least for four main reasons. Firstly, many existing communication and radar systems were developed independently and are not designed to be integrated into a single system. Therefore, there is a need to investigate coexistence mechanisms that enable communication and radar systems to operate without interfering with each other. Secondly, the radio spectrum is a scarce finite resource due to the growing demand for wireless communication. In many scenarios, it may not be feasible to allocate a separate band for ISAC systems. Therefore, coexistence mechanisms that allow communication and radar systems to share the same spectrum are of great interest. Thirdly, ISAC systems require complex hardware and software integration, including in some cases full-duplex circuitry, which can be challenging and expensive to implement, while coexistence mechanisms are generally less complex. Finally, in many scenarios, communication and radar systems may operate in the same frequency band and interfere with each other. Therefore, there is a need for interference management techniques that enable communication and radar systems to coexist in the same frequency band without compromising their performance.

Robust designs for ISAC systems are available in the literature. Specifically, some initial works have focused on developing robust design frameworks for joint radar-communication systems, including ISAC [25], [26], [27], [28]. These frameworks aim to ensure reliable and efficient operation of the combined radar-communication system in the presence of uncertainties and external disturbances. In [25], the authors proposed a spectrum sharing approach for wireless vehicle-to-vehicle (V2V) communication and automotive radar in intelligent transportation systems (ITS) to provide higher spectrum utilization efficiency. Additionally, the paper [26] proposed a robust and secure design for joint radar-communication systems, which integrates radar, communication, and jamming functionalities. In [27], instead, the authors proposed a robust beamforming design algorithm to achieve maximum secrecy rate for the multi-user downlink ISAC systems considering the probabilistic CSI uncertainty, where multiple targets also act as potential eavesdroppers. Furthermore, [28] presented a novel design approach and optimization framework for ISAC systems, where the available resources are jointly optimized over a sequence of variable-length snapshots.

In contrast to these existing works, our paper considers the robust RIS-aided radar-communication coexistence scenario where a statistical CSI error model is considered. The proposed design aims to ensure efficient and reliable operation of the RIS-aided radar-communication system in the presence of uncertainties and external disturbances. This work, thus, represents a significant contribution to the development of robust design frameworks for joint radar-communication systems, and can help to pave the way for future research in this area.

B. Main Contributions

In this paper, we consider a classical scenario where a pair of multi-antenna communication transmitter and receiver shares the same spectral band with a MIMO radar. Unlike the RIS-assisted system in [8] and the conventional system without RIS [3], we examine here multi-stream RIS-assisted MIMO communication-radar coexistence system, where the RIS helps in removing the generated mutual interference between the two systems, thus improving their coexistence. Specifically, the main contributions are summarized as follows.

- We propose a novel RIS-assisted radar communication coexistence framework. The design problem aims to maximize the radar SINR by jointly optimizing the active radar beamforming, the passive RIS beamforming, and communication transmitter covariance matrices under communication rate constraints, and communication and radar power budget constraints.
- The coexistence design problem is solved first under perfect direct and cascaded channel CSI. Alternating optimization is used to decouple the optimization problem and divide it into three separate sub-problems. The communication covariance optimization sub-problem is solved using Lagrangian dual decomposition. The radar active beamforming sub-problem is solved using the successive convex programming approach. Finally, the RIS passive beamforming sub-problem is solved through a linear local search method.
- We extend the coexistence design problem to the robust case where we consider a statistical CSI error model and solve the design problem by following the same approach used for the perfect CSI case.
- Simulation results are presented to validate our analysis and verify the effectiveness of the proposed RIS-assisted radar communication coexistence design with both perfect CSI and CSI uncertainty cases.

C. Organization

This paper is organized as follows. **Section** II introduces the coexistence system model. In **Section** III, we formulate the coexistence optimization problem and develop an alternating optimization based solution with perfect CSI. The robust coexistence design for imperfect CSI is presented in **Section** IV. In **Section** V provides a detailed discussion about the complexity, convergence, and optimality of the provided solutions in both full CSI and statistical CSI scenarios. Simulation results are presented and discussed in **Section** VI, while, finally, concluding remarks are given in **Section** VII.

Notations: In the following, $\mathbb{R}$, $\mathbb{C}$, and $\mathbb{N}$ denote the set of real, complex and natural numbers, respectively, while i is the imaginary unit; vectors and matrices are denoted by lowercase and uppercase boldface letters, respectively; $\mathbf{X} \succ \mathbf{0}$ and $\mathbf{X} \succeq \mathbf{0}$, means that the matrix $\mathbf{X}$ is Hermitian positive definite and positive semidefinite, respectively; $[.]^*$, $[.]^T$, $[.]^H$, and $(.)^{-1}$ are used to refer to the complex conjugate, transpose, conjugate-transpose, and the inversion operations, respectively; $\mathbf{I}_n$ is the $n \times n$ identity matrix; $\mathbf{0}_n$ is the all-zero n-dimensional column vector; $\mathbf{0}_{m,n}$ is the $m \times n$ with all zero entries; $\text{diag}\,(a_1, \cdots a_n)$ is the $n \times n$ diagonal matrix with entries $\{a_i\}_{i=1}^n$ on the principal diagonal; $\mathbf{X}^{1/2}$ is the square root matrix of $\mathbf{X} \succeq 0$; $\text{Tr}(.)$, $|.|$, and $\|.\|_F$ denote the trace, the determinant, and the Frobenius norm of its matrix argument; $\text{Re}\{.\}$ expresses the real value of its complex argument; Finally, $\text{diag}(\mathbf{A})$ and $\mathbb{E}\{\cdot\}$ outputs a vector containing the diagonal elements of a matrix $\mathbf{A}$ and the expected value of its argument.

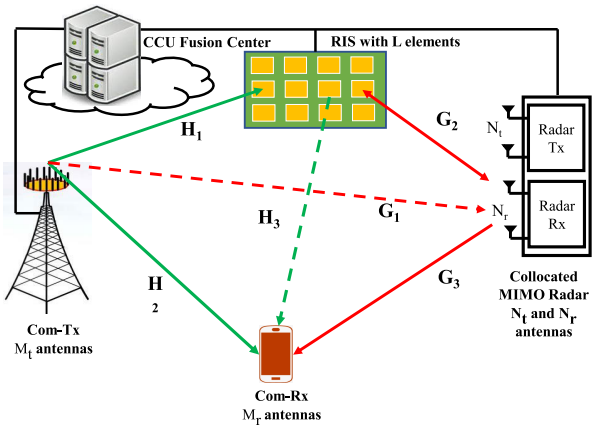

Fig. 1. The considered system model.

II. System Model

Consider a spectrum sharing problem between a MIMO radar and a MIMO communication system where both systems are assisted by an RIS, as shown in Fig. 1. Specifically, an $\text{M}_\text{t}-$antennas communication transmitter is communicating with an M_r-antennas receiver, sharing the same spectrum bands assigned to a MIMO radar system with N antennas at its transceiver arranged as a uniform linear array (ULA) with inter-element spacing d. The MIMO radar is pulse-based and used to detect K far-field point targets, with pulse repetition interval (PRI) T_{PRI} and carrier wavelength λ_c. Adopting pulsed radars for target sensing and ranging in both stand-alone radars and integrated radar communication systems brings some key advantages. For instance, they are able to distinguish between targets that are close together in range due to their high range resolution capability. Additionally, pulsed radars are able to use pulse compression techniques to increase their capability to detect targets in noisy environments. Furthermore, pulsed radars can also provide high Doppler sensitivity; finally, a pulsed radar typically consumes less power than other radar types, such as continuous wave (CW) radar or frequency-modulated continuous wave (FMCW) radar, since the transmitter is only active during the transmission of the pulse. In this work, the targets are assumed to be at angles $\{\phi_k\}$, having target reflection coefficient $\{\beta_k\}$, and Doppler shifts $\{\nu_k\}$. Each element in the radar array transmits L_P pulses, and accordingly the waveform matrix of the MIMO radar signal is expressed as $\mathbf{S} = [\mathbf{s}(1), \cdots, \mathbf{s}(L_P)] \in \mathbb{C}^{N \times L_p}$ with $\mathbf{s}(l) = [s_1(l), \cdots, s_N(l)]^T$ being the l-th snapshot out of all antenna elements. Typically, the transmit waveforms are assumed to be orthogonal, *i.e.,* $\mathbf{S}\mathbf{S}^H = \mathbf{I}_N$. We denote by $\mathbf{H}_1 \in \mathbb{C}^{L_R \times M_t}$, $\mathbf{G}_1^H \in \mathbb{C}^{N \times M_t}$, and $\mathbf{H}_2^H \in \mathbb{C}^{M_r \times M_t}$, the baseband equivalent channels between the communication

transmitter and RIS, between the communication transmitter and radar, and between the communication transmitter and its receiver, respectively. Additionally, the baseband equivalent channels between radar and RIS, and between radar and communication receiver are denoted as $\mathbf{G}_2^H \in \mathbb{C}^{N\times L_R}$, and $\mathbf{G}_3^H \in \mathbb{C}^{M_r\times N}$, respectively. Finally, the baseband equivalent channel between the RIS and the communication receiver is denoted as $\mathbf{H}_3 \in \mathbb{C}^{M_r\times L_R}$. For all previously mentioned channels, a block-fading channel model is assumed.

In order to enable coexistence between the two systems, an RIS with $\mathrm{L_R}$ reflecting elements is deployed to improve the target detection probability of the radar system, and the spectral efficiency of the communication system. In the context of systems coexistence, coordination means that active systems cooperate to negotiate their transmit policies and adjust their detection/demodulation strategies. This is done through co-design, which involves the joint design of radar waveforms and communication system codebooks to preserve the performance of both systems while allowing for coexistence. To achieve this, the following steps can be taken: conduct a spectrum analysis, establish coordination protocols, place antennas in a way that minimizes interference, use filters to limit unwanted transmissions, and use adaptive techniques to adjust parameters dynamically. By following these steps, full coordination between radar and communication systems can be achieved, enabling them to operate without interference. To maintain coordination between MIMO radar and MIMO communication systems, a central control unit (CCU) can be implemented and connected to the RIS. The CCU is functionally integrated with the radar fusion center and has high computational capabilities to implement the proposed spectrum sharing framework. It collects relevant data, uses the framework to compute design configurations, and distributes these configurations to the corresponding systems. [19].

Let us now denote by $\mathbf{Y}_R$ the $N \times L_P$ matrix whose l-th column contains the signal received at the MIMO radar during the l-the communication symbol interval, with one PRI spanning L_P communication symbol intervals. Also, let $\mathbf{\Theta} \in \mathbb{C}^{L_R\times L_R} \triangleq \mathrm{diag}\left(\theta_1,\cdots,\theta_{L_R}\right)$ denote the RIS phase shifts matrix, where $\theta_l = \beta_l e^{j\psi_l}$ represents the reflecting coefficient for the $l-$th RIS element. As it happens in practice, a discrete phase shift model is considered, in which $\psi_l \in \mathcal{F}_l = \{\psi_{1,l},\dots\psi_{J,l}\}$, with $\psi_{j,l}$ the j-th discrete level that the phase shift ψ_l can take. Moreover, the realistic scenario in which the modulus and phase of each RIS reflection coefficient are mutually dependent is here considered. Specifically, the following expression links β_l and ψ_l for any $l = 1,\dots,L_R$ [29]: $\beta_l\left(\psi_l\right) = \left(1-\kappa_{\min}\right)\left(\frac{\sin(\psi_l-\varphi)+1}{2}\right)^{\alpha}+\kappa_{\min}$, where $\kappa_{\min}>0$ is the minimum available amplitude, $\varphi>0$ is the horizontal distance between $-\pi/2$ and κ_{min}, while α is the steepness of the function curve. Next, we denote by $\mathbf{X}$ the communication signal matrix, with its columns as codewords from the communication system code-book. Based on the scenario shown in Fig. 1, and letting $\mathbf{W}_R$ be the additive white Gaussian noise at the MIMO radar receiver, it holds that:

$$\mathbf{Y}_R = \mathbf{V}_r\mathbf{\Sigma}\mathbf{V}_t^T\mathbf{F}\mathbf{S} + \left(\mathbf{G}_1^H + \mathbf{G}_2^H\mathbf{\Theta}^H\mathbf{H}_1\right)\mathbf{X} + \mathbf{W}_R, \quad (1)$$

where $\mathbf{F} \in \mathbb{C}^{N\times N}$ is the transmit beamforming matrix at the MIMO radar transmitter, while $\mathbf{V}_r$ and $\mathbf{V}_t$ are the transmit and receive steering matrices of the MIMO radar towards the K targets, namely $\mathbf{V}_t \triangleq [\mathbf{v}_t(\phi_1),\cdots,\mathbf{v}_t(\phi_K)]$, $\mathbf{V}_r \triangleq \left[\mathbf{v}_r(\phi_1),\cdots,\mathbf{v}_r(\phi_K)\right]$, wherein

$$\mathbf{v}_t(\phi_k) \triangleq \mathbf{v}_r(\phi_k) = \left[1, \mathrm{e}^{\frac{-j2\pi \mathrm{d}\sin(\phi_k)}{\lambda_c}},\cdots,\mathrm{e}^{\frac{-j2\pi(N-1)d\sin(\phi_k)}{\lambda_c}}\right]^T, \quad (2)$$

and $\mathbf{\Sigma} \triangleq diag\left(\left[\rho_1\mathrm{e}^{j2\pi\nu_1},\cdots,\rho_K\mathrm{e}^{j2\pi\nu_K}\right]\right)$. For convenience, let us also denote by $\mathbf{D} \triangleq \mathbf{V}_r\mathbf{\Sigma}\mathbf{V}_t^T$ the target response matrix. The matrix $\mathbf{Y}_R$ is then forwarded to the fusion center to carry out target estimation.

On the other hand, the baseband signal at the MIMO communication receiver during one PRI is given by:

$$\mathbf{Y}_C = \left(\mathbf{H}_2^H + \mathbf{H}_3^H\mathbf{\Theta}^H\mathbf{H}_1\right)\mathbf{X} + \left(\mathbf{G}_3^H + \mathbf{H}_3^H\mathbf{\Theta}^H\mathbf{G}_2\right)\mathbf{F}\mathbf{S} + \mathbf{W}_C, \quad (3)$$

with $\mathbf{W}_C$ the white additive Gaussian noise at the communication receiver. The two following CSI assumptions and problem statements will be considered in this paper:

- **Perfect CSI**: all channels are reliably estimated in each channel coherence time and their estimates are used for resource allocation purposes. This case is addressed in Section III.
- **Statistical CSI**: a statistical mean feedback model is assumed for the channel from the RIS to the mobile user, while all other channels are reliably estimated. This scenario is motivated by the consideration that a passive RIS has no transmission or signal processing capabilities. Thus, estimating at the transmitter the channel from the RIS to the mobile terminal is problematic, and it is assumed here that only the distribution, mean, and covariance matrix of the channel from the RIS to the mobile user are known. On the other hand, estimating the channels $\mathbf{H}_1$ and $\mathbf{G}_2$ is realistic since the base station, RIS, and radar transceiver are fixed network nodes. As for the other channels, they do not involve the RIS and thus can be estimated by conventional techniques. This case is treated in Section IV.

III. System Design With Perfect CSI

To begin with, let us first derive mathematical expressions for the radar SINR and the communication rate in order to formulate the problem, and then turn to the proposed solution technique.

A. Problem Formulation With Perfect CSI

The covariance matrix of the interference plus noise term can be expressed as:

$$\begin{aligned}\mathbf{Q}_{\mathrm{Cin}} &= \left(\mathbf{G}_3^H+\mathbf{H}_3^H\mathbf{\Theta}^H\mathbf{G}_2\right)\mathbf{\Phi}\left(\mathbf{G}_3^H+\mathbf{H}_3^H\mathbf{\Theta}^H\mathbf{G}_2\right)^H+\sigma_C^2\mathbf{I}\\ &= \mathbf{G}_{\mathrm{eff}}\,\mathbf{\Phi}\,\mathbf{G}_{\mathrm{eff}}^H+\sigma_C^2\mathbf{I}\end{aligned} \quad (4)$$

where $\mathbf{G}_{\mathrm{eff}} = \mathbf{G}_3^H + \mathbf{H}_3^H\mathbf{\Theta}^H\,\mathbf{G}_2$, and $\mathbf{\Phi} \triangleq \mathbf{F}\mathbf{F}^H/L_P$. If the codeword $\mathbf{x}(l)$, $l \in \mathbb{N}_{L_P}^+$ is distributed as $\mathcal{CN}\left(0,\mathbf{Q}_{\mathrm{xl}}\right)$,

then the average sum-rate for the communication system over a time frame of L_P symbols is $C_{\text{avg}}\left(\boldsymbol{\Theta}, \mathbf{Q}_{\text{xl}}, \boldsymbol{\Phi}\right) \triangleq \frac{1}{L_P}\sum_{l=1}^{L_P} C\left(\mathbf{Q}_{\text{xl}}, \boldsymbol{\Theta}, \boldsymbol{\Phi}\right)$, where $C\left(\boldsymbol{\Theta}, \mathbf{Q}_{\text{xl}}, \boldsymbol{\Phi}\right)$ is the communication rate achieved with the codeword $\mathbf{x}(l)$, $l \in \mathcal{N}_{L_P}^{+}$, and is expressed as

$$C\left(\boldsymbol{\Theta}, \mathbf{Q}_{\text{xl}}, \boldsymbol{\Phi}\right) \triangleq \log_2 \left|\mathbf{I} + \mathbf{Q}_{\text{Cin}}^{-1}\, \mathbf{H}_{\text{eff}}\, \mathbf{Q}_{\text{xl}}\, \mathbf{H}_{\text{eff}}^{H}\right|, \quad (5)$$

with $\mathbf{H}_{\text{eff}} = \left(\mathbf{H}_2^H + \mathbf{H}_3^H \boldsymbol{\Theta}^H \mathbf{H}_1\right)$.

Next, as for the radar system, based on (1)-(2), the received signal power (RSP) at the radar receiver can be computed as

$$\begin{aligned}
\text{RSP} &\triangleq \mathbb{E}\left\{\text{Tr}\left(\left(\mathbf{DFS}\right)\left(\mathbf{DFS}\right)^H\right)\right\} \\
&= \mathbb{E}\left\{\text{Tr}\left\{\sum_k \sum_j \beta_k \beta_j \left(\mathbf{D}_k \mathbf{FS}\right)\left(\mathbf{D}_j \mathbf{FS}\right)^H\right\}\right\} \\
&\overset{(a)}{=} \text{Tr}\left\{L_P \sum_k \sigma_{\beta_k}^2 \left[\mathbf{D}_k \boldsymbol{\Phi} \mathbf{D}_k^H\right]\right\} \\
&= \text{Tr}\left\{L_P \boldsymbol{\Phi} \sum_k \sigma_{\beta_k}^2 \mathbf{v}_t^*(\phi_k)\, \mathbf{v}_r^H(\phi_k)\, \mathbf{v}_r(\phi_k)\, \mathbf{v}_t^T(\phi_k)\right\} \\
&\overset{(b)}{=} L_P\, N\, \text{Tr}\left(\boldsymbol{\Phi} \sum_k \sigma_{\beta_k}^2 \mathbf{v}_t^*(\phi_k)\, \mathbf{v}_t^T(\phi_k)\right) \\
&= L_P N\, \text{Tr}\left(\boldsymbol{\Phi} \mathbf{D}_t\right), \qquad (6)
\end{aligned}$$

where $\mathbf{D}_k \triangleq \mathbf{v}_r\left(\phi_k\right)\mathbf{v}_t^T\left(\phi_k\right)$, $\mathbf{s}_l \triangleq \mathbf{s}(l)$, $\mathbf{D}_t = \sum_k \sigma_{\beta_k}^2 \mathbf{v}_t^*(\phi_k)\, \mathbf{v}_t^T(\phi_k)$, and (a) follows from the fact that $\mathbb{E}\left\{\beta_k \beta_j\right\} = \delta_{jk}\sigma_{\beta_k}^2$ and when $k = j$, this leads to $\mathbb{E}\left\{\beta_k \beta_{j=k}\right\} = \sigma_{\beta_k}^2$, and $\mathbf{F}\mathbf{F}^H = L_P \boldsymbol{\Phi}$, while (b) follows from the fact that $\mathbf{v}_r^H(\phi_k)\mathbf{v}_r(\phi_k) = L_P N$.

By following similar steps, the power of the interference signal received at the radar receiver can be derived as follows

$$\begin{aligned}
\text{RIP} &\triangleq \text{Tr}\left(\left(\mathbf{G}_1^H + \mathbf{G}_2^H \boldsymbol{\Theta}^H \mathbf{H}_1\right) \mathbf{Q}_{\text{xl}} \left(\mathbf{G}_1^H + \mathbf{G}_2^H \boldsymbol{\Theta}^H \mathbf{H}_1\right)^H\right) \\
&= \text{Tr}\left(\mathbf{G}_{\text{eff}}\, \mathbf{Q}_{\text{xl}}\, \mathbf{G}_{\text{eff}}^H\right) \qquad (7)
\end{aligned}$$

where $\mathbf{Q}_{\text{xl}}$ denotes the interference covariance matrix of the radar sensing waveform for all $l \in \mathbb{N}_{L_P}^{+}$. Then, based on (6) and (7), the signal to interference plus noise ratio (SINR) at the radar receiver can be finally written as

$$\text{SINR} = \frac{\text{Tr}\left(\boldsymbol{\Phi}\mathbf{D}_t\right)}{\frac{1}{N}\text{Tr}\left(\mathbf{G}_{\text{eff}} \mathbf{Q}_{\text{xl}} \mathbf{G}_{\text{eff}}^H\right) + \sigma_R^2}. \quad (8)$$

We consider thus the following problem:

$$\begin{aligned}
&\max_{\boldsymbol{\Theta}, \mathbf{Q}_{\text{xl}}, \boldsymbol{\Phi}} \quad \text{SINR}\left(\boldsymbol{\Theta}, \mathbf{Q}_{\text{xl}}, \boldsymbol{\Phi}\right) && (9a) \\
&\text{Subject to:} \quad C\Big(\boldsymbol{\Theta}, \mathbf{Q}_{\text{xl}}, \boldsymbol{\Phi}\Big) \geq C_{\text{th}}, && (9b) \\
&\qquad L_P\, \text{Tr}\left(\mathbf{Q}_{\text{xl}}\right) \leq P_C, \quad L_P\, \text{Tr}\left(\boldsymbol{\Phi}\right) \leq P_R, && (9c) \\
&\qquad \text{Tr}\left(\boldsymbol{\Phi}\mathbf{V}_k\right) \geq \zeta\, \text{Tr}\left(\boldsymbol{\Phi}\right), \quad \forall k \in \mathbb{N}_K^{+}, && (9d) \\
&\qquad \theta_l \in \mathcal{F}_l, \forall l = 1, \cdots, L_R, && (9e)
\end{aligned}$$

with $\mathbf{V}_k \triangleq \mathbf{v}_t^*(\phi_k)\mathbf{v}_t^T(\phi_k)$. The constraint in (9b) represents the quality of service rate constraint of the communication link, *i.e.,* the communication rate cannot be smaller than C_{th}. The first and second part of the constraint in (9c) set the power budget for the communication and radar systems, respectively. The constraint in (9d) keeps the power of the radar waveform in the directions of interest at least at the level achieved with the use of a uniform precoding matrix, i.e. $\frac{\text{Tr}(\boldsymbol{\Phi})}{N}\mathbf{I}$. This constraint is derived as $\mathbf{v}_t^T(\phi_k)\boldsymbol{\Phi}\mathbf{v}_t^*(\phi_k) \geq \zeta \mathbf{v}_t^T(\phi_k)\frac{\text{Tr}(\boldsymbol{\Phi})}{N}\mathbf{I}\mathbf{v}_t^*(\phi_k) = \zeta\, \text{Tr}(\boldsymbol{\Phi})$, and the value of $\zeta \geq 1$ is used to design the beampattern at the target angles of interest [30], [33]. The constraint in (9e) accounts for the feasible values of the reflection coefficients of the RIS reflecting elements [8].

B. Alternating Optimization Based Solution to (9)

Problem (9) can be seen to be non-convex with respect to the optimization parameters $(\boldsymbol{\Theta}, \mathbf{Q}_{\text{xl}}, \boldsymbol{\Phi})$. Moreover, the fact that discrete reflection coefficients levels are considered further complicates its solution. To tackle Problem (9), a convenient approach is thus to employ the alternating maximization algorithm, which decouples the problem into three sub-problems for the three optimization variables $(\boldsymbol{\Theta}, \mathbf{Q}_{\text{xl}}, \boldsymbol{\Phi})$. The optimization of the three variable blocks $(\boldsymbol{\Theta}, \mathbf{Q}_{\text{xl}}, \boldsymbol{\Phi})$ is addressed in the rest of this section.

*1) **Optimization With Respect to** $\mathbf{Q}_{\text{xl}}$:* When $\boldsymbol{\Theta}$ and $\boldsymbol{\Phi}$ are fixed, the optimization of $\mathbf{Q}_{\text{xl}}$ amounts to solving the minimization problem

$$\min_{\mathbf{Q}_{\text{xl}} \succeq 0} \text{Tr}\Big(\left(\mathbf{G}_1^H + \mathbf{G}_2^H \boldsymbol{\Theta}^H \mathbf{H}_1\right)\mathbf{Q}_{\text{xl}}\left(\mathbf{G}_1^H + \mathbf{G}_2^H \boldsymbol{\Theta}^H \mathbf{H}_1\right)^H\Big) \quad (10a)$$

$$\text{S. t.} \quad C_{\text{avg}}\Big(\boldsymbol{\Theta}, \mathbf{Q}_{\text{xl}}, \boldsymbol{\Phi}\Big) \geq C_{\text{th}}, \quad (10b)$$

$$\text{Tr}\left(\mathbf{Q}_{\text{xl}}\right) \leq P_C/L_P\,. \quad (10c)$$

Problem (10) is jointly convex with respect to the variables $\{\mathbf{Q}_{\text{xl}}\}$. Indeed, the objective and constraint function in (10c) are linear, while the constraint in (10b) is concave. Thus, Problem (10) can be solved by means of convex optimization theory, with affordable complexity.

*2) **Optimization With Respect to** $\boldsymbol{\Phi}$:* When $\mathbf{Q}_{\text{xl}}$ and $\boldsymbol{\Theta}$ are fixed, the optimization of $\boldsymbol{\Phi}$ amounts to solving

$$\begin{aligned}
&\max_{\boldsymbol{\Phi} \succeq 0} \quad \text{Tr}\left(\boldsymbol{\Phi}\mathbf{D}_t\right) && (11a) \\
&\text{S. t.} \quad C_{\text{avg}}\Big(\boldsymbol{\Theta}, \mathbf{Q}_{\text{xl}}, \boldsymbol{\Phi}\Big) \geq C_{\text{th}}, && (11b) \\
&\qquad \text{Tr}\left(\boldsymbol{\Phi}\right) \leq P_R/L_P, && (11c) \\
&\qquad \text{Tr}\left(\boldsymbol{\Phi}\mathbf{V}_k\right) \geq \zeta\, \text{Tr}\left(\boldsymbol{\Phi}\right), \quad \forall k \in \mathbb{N}_K^{+}, && (11d)
\end{aligned}$$

The difficulty in solving Problem (11) lies in Constraint (11b), because C_{avg} is not a concave function of $\boldsymbol{\Phi}$. In fact, C_{avg} can be seen to be a convex function of $\boldsymbol{\Phi}$. However, the convexity of (11b) also provides a way of tackling Problem (11), by resorting to the sequential programming framework. Indeed, since (11b) is a convex function, it is possible to lower-bound C_{avg} by its first-order Taylor expansion around any point $\bar{\boldsymbol{\Phi}}$, namely,

$$\begin{aligned}
C_{\text{avg}}\Big(\boldsymbol{\Theta}, \mathbf{Q}_{\text{xl}}, \boldsymbol{\Phi}\Big) &\geq C_{\text{avg}}\Big(\boldsymbol{\Theta}, \mathbf{Q}_{\text{xl}}, \bar{\boldsymbol{\Phi}}\Big) \qquad (12) \\
&\quad - \text{Tr}\left[\text{Re}\left\{\frac{1}{L_p}\sum_{l=1}^{L_P} \mathbf{F}_l^H\left(\boldsymbol{\Phi} - \bar{\boldsymbol{\Phi}}\right)\right\}\right] \\
&= \tilde{C}\Big(\boldsymbol{\Theta}, \mathbf{Q}_{\text{xl}}, \boldsymbol{\Phi}\Big), \qquad (13)
\end{aligned}$$

where $\mathbf{F}_l$ is given as

$$\begin{aligned}\mathbf{F}_l &\cong -\left(\frac{\partial C\left(\boldsymbol{\Theta}, \mathbf{Q}_{\mathrm{xl}}, \boldsymbol{\Phi}\right)}{\partial \mathrm{Re}\{\boldsymbol{\Phi}\}}\right)^T_{\boldsymbol{\Phi}=\bar{\boldsymbol{\Phi}}} \\ &= \frac{\mathbf{G}_{\mathrm{eff}}^H}{\ln 2}\Big[\left(\mathbf{G}_{\mathrm{eff}}\boldsymbol{\Phi}\mathbf{G}_{\mathrm{eff}}^H + \sigma_C^2\mathbf{I}\right)^{-1} - \left(\mathbf{G}_{\mathrm{eff}}\boldsymbol{\Phi}\mathbf{G}_{\mathrm{eff}}^H \right. \\ &\qquad \left. + \sigma_C^2\mathbf{I} + \mathbf{H}_{\mathrm{eff}}\mathbf{Q}_{\mathrm{xl}}\mathbf{H}_{\mathrm{eff}}^H\right)^{-1}\Big]\mathbf{G}_{\mathrm{eff}} \end{aligned} \tag{14}$$

Then, Problem (11) can be tackled by the sequential programming framework, by solving, in each iteration the problem obtained from (11) by replacing Constraint (11b) with the right-hand-side of (12), which yields

$$\max_{\boldsymbol{\Phi} \succeq 0} \mathrm{Tr}\left(\boldsymbol{\Phi}\mathbf{D}_t\right) \tag{15a}$$

$$\text{s.t. } \tilde{C}\Big(\boldsymbol{\Theta}, \mathbf{Q}_{\mathrm{xl}}, \boldsymbol{\Phi}\Big) \geq C_{\mathrm{th}} \tag{15b}$$

$$\mathrm{Tr}\left(\boldsymbol{\Phi}\right) \leq P_R/L_P, \tag{15c}$$

$$\mathrm{Tr}\left(\boldsymbol{\Phi}\mathbf{V}_k\right) \geq \zeta\,\mathrm{Tr}\left(\boldsymbol{\Phi}\right), \quad \forall k \in \mathbb{N}_K^+, \tag{15d}$$

where $\mathbf{F} = \sum_{l=1}^{L_P}\mathbf{F}_l$, with $\mathbf{F}_l$ given by (14). In each iteration of the sequential method, $\bar{\boldsymbol{\Phi}}$ takes the optimized value of $\boldsymbol{\Phi}$ from the previous iteration. Problem (15) is linear in $\boldsymbol{\Phi}$, and thus can be solved by standard interior point approaches with a complexity of $\mathcal{O}((L_P N^2)^{3.5})$.

*3) **Optimization With Respect to** $\boldsymbol{\Theta}$:* If $\{\mathbf{Q}_{\mathrm{xl}}\}$ and $\boldsymbol{\Phi}$ are fixed, the optimization of $\boldsymbol{\Theta}$ is:

$$\min_{\boldsymbol{\Theta}} \ \mathrm{Tr}\left(\left(\mathbf{G}_1^H + \mathbf{G}_2^H\boldsymbol{\Theta}^H\mathbf{H}_1\right)\mathbf{Q}_{\mathrm{xl}}\left(\mathbf{G}_1^H + \mathbf{G}_2^H\boldsymbol{\Theta}^H\mathbf{H}_1\right)^H\right) \tag{16a}$$

$$\text{s. t. } C_{\mathrm{avg}}\Big(\boldsymbol{\Theta}, \mathbf{Q}_{\mathrm{xl}}, \boldsymbol{\Phi}\Big\}\Big) \geq C_{\mathrm{th}}, \tag{16b}$$

$$\theta_l \in \mathcal{F}, \mathcal{F} \triangleq \{\phi_l \mid |\phi_l| = 1\} \forall l = 1, \cdots, L_R, \tag{16c}$$

Problem (16) is not convex, because (16a) and (16b) are not concave with respect to $\boldsymbol{\Theta}$, and the matrix $\boldsymbol{\Theta}$ has discrete components which depend on the quantization bits representing the phase shift of each RIS element.

A computationally convenient way of tackling (16) is to optimize one RIS phase at a time, searching among all available discrete phase shifts. The details of the approach are given in Algorithm (1). Specifically, Algorithm (1) chooses the optimum value of the phase shift for each element, while keeping the remaining $N-1$ phase shifts of other elements constant, by traversing all the possible values, specified by the number of quantization bits, and then selecting the optimum one without violating the constraint (16b). Thus, the obtained optimum phase shift of a specific elements is used as constant while optimizing the phase shift for another element. This procedure continues until convergence.

While the proposed approach has the advantage of having a linear complexity in the number of RIS phase shifts and is able to provide the solution directly in the discrete angle domain, it can not guarantee convergence to the globally optimal solution. In the following we also develop, as a benchmark scheme, a relaxation and projection method, which works in three steps. First, the discrete phase shifts are relaxed to continuous variables in $[0, 2\pi]$. Second, the continuous-valued problem is solved by means of a standard gradient search, and then the optimized continuous phase shift values are projected onto the original discrete feasible set. The steps of the algorithm are summarized in Algorithm 2.

Algorithm 1 Linear Local Search for Phase Shifts Design

1: **Initialization:** The number of angles quantization bits b.
2: **Optimization Output:** $\boldsymbol{\Theta}^\star = diag\left(\theta_1^\star, \cdots, \theta_{L_R}^\star\right)$.
3: **for** $l = 1 : L_R$ **do**
4: Evaluate all the possible values based on the number of quantization bits b.
5: For all possible values θ_l, choose the value minimizing the objective of (16), while satisfying constraint (16b), denote it $\theta_l^\star$.
6: $\theta_l = \theta_l^\star$
7: **end for**

Algorithm 2 Relaxation and Projection Method for RIS Design

1: **Initialization:** Set the values of different channels.
2: **Optimization Output:** $\boldsymbol{\Theta}^*$
3: Relax the RIS phases ψ_l to continuous values in $[0, 2\pi]$, for all $l = 1, \ldots, L_R$;
4: Solve the relaxed optimization problem by gradient search to obtain $\boldsymbol{\Theta}_c = \mathrm{diag}(\psi_1, \ldots, \psi_{L_R})$;
5: Project ψ_l onto $\mathcal{F}_l$, for all $l = 1, \ldots, L_R$ to obtain $\boldsymbol{\Theta}^*$.

The difference between local search and relaxation and projection methods for phase shift optimization of the RIS can be explained as follows. Local search method is a type of optimization algorithm that starts with an initial solution and then iteratively improves it by exploring neighboring solutions until a stopping criterion is met. The relaxation and projection method, instead, is a type of projection gradient optimization algorithm that involves iteratively updating the solution by taking a step in the direction of the negative gradient of the objective function while projecting the solution onto a feasible set. While the proposed relaxation and projection algorithm has been included as a benchmark algorithm for comparison purposes, it cannot guarantee the attainment of the global optimum solution. The reason behind that is due to the relaxation of the original discrete optimization problem to a continuous one and then projecting the obtained solution from this continuous optimization problem onto the feasible set of phase shifts based on the used resolution setup. It is worth noting that developing alternative approaches that can achieve a global optimum solution while considering the constraints of the problem is still an open problem and active area of research.

With regard to the complexity of the two algorithms, for the linear search algorithm the complexity is linear with respect to both the number of RIS elements and the number of available angle choices. This means that the time and memory required by the algorithm increases linearly as the number of RIS elements and the resolution bits increase. Specifically, the time complexity of the linear search algorithm is $O(N \times 2^b)$, where

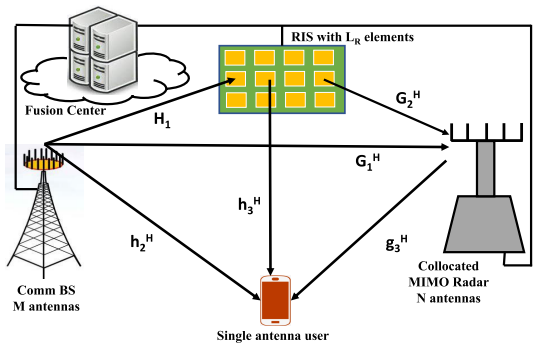

Fig. 2. The considered system model for the case of imperfect CSI.

N is the number of RIS elements and b is the number of resolution bits.

For the projected gradient algorithm, instead, the complexity depends on the optimization problem being solved. In general, it tends to have a higher complexity than the linear search algorithm, since the projected gradient algorithm requires the solution of an optimization problem at each iteration, which can be computationally expensive. Therefore the linear search algorithm usually has a lower computational complexity than the projected gradient algorithm.

IV. System Design With Statistical CSI

This section addresses the case in which only statistical CSI is available for the channel between the RIS and the mobile terminal. This assumption is considered due to the constrained power budget of the two end nodes involved in the channel $\mathbf{h}_3$, specifically the RIS and the user. Given such power constraint, traditional channel estimation techniques such as pilot-based estimation, least squares, maximum likelihood estimation, or even compressed sensing-based estimation are hardly viable in this particular channel. However, it is important to note that these estimation methods can still be employed for other channels within the context illustrated in Figure 2. It is essential to highlight that statistical CSI characterizes the average behavior of the channel over a defined time period or frequency range. It is typically estimated by observing numerous realizations of the channel and is utilized to optimize system design and performance over an extended duration. For mathematical tractability reasons, in this section we assume that the mobile terminal is equipped with a single antenna, and we denote by $\mathbf{h}_3$ the vector channel from the RIS to the mobile terminal. A mean covariance feedback model is considered, according to which the imperfectly known channel is modeled as $\mathbf{h}_3 = \widehat{\mathbf{h}}_3 + \Delta\mathbf{h}_3$, with $\Delta\mathbf{h}_3$ being distributed as a random complex Gaussian vector with zero mean and covariance matrix $\mathbf{\Sigma}_{h_3}$, while the instantaneous realization of $\mathbf{h}_3$ is not available. Thus, $\widehat{\mathbf{h}}_3$ represent the mean of the random vector $\mathbf{h}_3$. The choice of a Gaussian distribution is realistic in practical scenarios [34]. The new system model is depicted in Fig. 2.

Given the random vector $\mathbf{h}_3$, the received signals at the communication user and at the radar receiver are expressed as

$$y_c = \left(\mathbf{h}_2^H + \mathbf{h}_3^H\mathbf{\Theta}^H\mathbf{H}_1\right)\mathbf{t}x \tag{17}$$

$$+ \sqrt{P_R}\left(\mathbf{g}_3^H + \mathbf{h}_3^H\mathbf{\Theta}^H\mathbf{G}_2\right)\mathbf{F}\mathbf{s} + w_c\,,$$
$$\mathbf{y}_R = \alpha\sqrt{P_R}\mathbf{V}_r\mathbf{\Sigma}\mathbf{V}_t^T\mathbf{F}\mathbf{s} + \left(\mathbf{G}_1^H + \mathbf{G}_2^H\mathbf{\Theta}^H\mathbf{H}_1\right)\mathbf{t}x + \mathbf{w}_r\,, \tag{18}$$

respectively, where x represent the communication symbol to be transmitted from the BS to the user. The vector $\mathbf{t}$ and the matrix $\mathbf{F}$ represent the beamformers used at the BS and at the radar, respectively. The SINR at the mobile user can be thus be expressed as:

$$\gamma_c = \frac{|\tilde{\mathbf{h}}_2^H\,\mathbf{t}|^2}{L_P P_R \tilde{\mathbf{g}}_3^H\mathbf{\Phi}\tilde{\mathbf{g}}_3 + \sigma_c^2} \tag{19}$$

where $\tilde{\mathbf{h}}_2^H$ and $\tilde{\mathbf{g}}_3^H$ are the composite channels $\left(\mathbf{h}_2^H + \mathbf{h}_3^H\mathbf{\Theta}^H\mathbf{H}_1\right)$ and $\left(\mathbf{g}_3^H + \mathbf{h}_3^H\mathbf{\Theta}^H\mathbf{G}_2\right)$, respectively, and we recall that $\mathbf{\Phi} = \mathbf{F}\mathbf{F}^H/L_P$. As a consequence, the achievable rate of the mobile user can be expressed as:

$$\mathcal{C}\left(\mathbf{t}, \mathbf{\Theta}, \mathbf{\Phi}\right) = \log_2\left(1 + \frac{|\tilde{\mathbf{h}}_2^H\,\mathbf{t}|^2}{L_P P_R \tilde{\mathbf{g}}_3^H\mathbf{\Phi}\tilde{\mathbf{g}}_3 + \sigma_c^2}\right) \tag{20}$$

Denoting the maximum data rate outage probability as $\rho \in (0, 1]$, the considered design optimization problem consists on the maximization of the average SINR at the mobile user, subject to an outage constraint at the mobile user, and to the same power constraints and quality-of-service constraints for the radar receiver as in the perfect CSI scenario:

$$\max_{\mathbf{\Phi},\mathbf{e},\mathbf{t}} \quad \frac{\mathbb{E}\left[|\tilde{\mathbf{h}}_2^H\mathbf{t}|^2\right]}{L_P P_R \mathbb{E}\left[\tilde{\mathbf{g}}_3^H\mathbf{\Phi}\tilde{\mathbf{g}}_3\right] + \sigma_c^2} \tag{21a}$$
$$\text{Subject to:} \quad \Pr\left\{C\left(\mathbf{\Phi}, \mathbf{\Theta}, \mathbf{t}\right) \geq C_{\text{th}}\right\} \geq 1 - \rho, \tag{21b}$$
$$L_P\|\mathbf{t}\|^H \leq P_C \tag{21c}$$
$$(9d),\ (9e) \tag{21d}$$

wherein the rate outage constraint (21b) guarantees the maximum outage probability. The challenge in tackling Problem (21) lies in evaluating both the statistical expectations in the objective (21a) and in the outage probability in (21b).

As for the objective function, the statistical expectations can be evaluated as follows:

$$\begin{aligned}
&\mathbb{E}\left[|\tilde{\mathbf{h}}_2^H\mathbf{t}|^2\right] \\
&= \mathbf{t}^H\mathbb{E}\left[\left(\mathbf{h}_2 + \mathbf{H}_1^H\mathbf{\Theta}\mathbf{h}_3\right)\left(\mathbf{h}_2 + \mathbf{H}_1^H\mathbf{\Theta}\mathbf{h}_3\right)^H\right]\mathbf{t} \\
&= \mathbf{t}^H\mathbf{h}_2\mathbf{h}_2^H\mathbf{t} + \mathbf{t}^H\mathbf{H}_1^H\mathbf{\Theta}\mathbb{E}\left[(\widehat{\mathbf{h}}_3 + \Delta\mathbf{h}_3)(\widehat{\mathbf{h}}_3 + \Delta\mathbf{h}_3)^H\right]\mathbf{\Theta}^H\mathbf{H}_1\mathbf{t} \\
&\quad + \mathbf{t}^H\left(\mathbf{h}_2\widehat{\mathbf{h}}_3^H\mathbf{\Theta}^H\mathbf{H}_1 + \mathbf{H}_1^H\mathbf{\Theta}\widehat{\mathbf{h}}_3\mathbf{h}_2^H\right)\mathbf{t} \qquad (22) \\
&= \left|\mathbf{t}^H\mathbf{h}_2\right|^2 + \mathbf{t}^H\mathbf{H}_1^H\mathbf{\Theta}\left(\widehat{\mathbf{h}}_3\widehat{\mathbf{h}}_3^H + \mathbb{E}\left[\Delta\mathbf{h}_3\Delta\mathbf{h}_3^H\right]\right)\mathbf{\Theta}^H\mathbf{H}_1\mathbf{t} \\
&\quad + \mathbf{t}^H\left(\mathbf{h}_2\widehat{\mathbf{h}}_3^H\mathbf{\Theta}^H\mathbf{H}_1 + \mathbf{H}_1^H\mathbf{\Theta}\widehat{\mathbf{h}}_3\mathbf{h}_2^H\right)\mathbf{t} \qquad (23) \\
&= \left|\mathbf{t}^H\mathbf{h}_2\right|^2 + \mathbf{t}^H\mathbf{H}_1^H\mathbf{\Theta}\left(\widehat{\mathbf{h}}_3\widehat{\mathbf{h}}_3^H + \mathbf{\Sigma}_{h_3}\right)\mathbf{\Theta}^H\mathbf{H}_1\mathbf{t} \\
&\quad + \mathbf{t}^H\left(\mathbf{h}_2\widehat{\mathbf{h}}_3^H\mathbf{\Theta}^H\mathbf{H}_1 + \mathbf{H}_1^H\mathbf{\Theta}\widehat{\mathbf{h}}_3\mathbf{h}_2^H\right)\mathbf{t}\,. \qquad (24)
\end{aligned}$$

$$\begin{aligned}
&\mathbb{E}\left[\tilde{\mathbf{g}}_3^H\mathbf{\Phi}\tilde{\mathbf{g}}_3\right] \\
&= \mathbb{E}\left[\text{tr}(\mathbf{\Phi}\tilde{\mathbf{g}}_3\tilde{\mathbf{g}}_3^H)\right] = \text{tr}(\mathbf{\Phi}\mathbb{E}\left[\tilde{\mathbf{g}}_3\tilde{\mathbf{g}}_3^H\right)] \\
&= \text{tr}\left(\mathbf{\Phi}\left(\mathbf{g}_3\mathbf{g}_3^H + \mathbf{G}_2^H\mathbf{\Theta}\left(\widehat{\mathbf{h}}_3\widehat{\mathbf{h}}_3^H + \mathbf{\Sigma}_{h_3}\right)\mathbf{\Theta}^H\mathbf{G}_2\right)\right)
\end{aligned}$$

$$= \mathbf{g}_3^H \mathbf{\Phi} \mathbf{g}_3 + \mathrm{tr}\left(\mathbf{\Phi}\mathbf{G}_2^H \mathbf{\Theta}\left(\widehat{\mathbf{h}}_3\widehat{\mathbf{h}}_3^H + \mathbf{\Sigma}_{h_3}\right)\mathbf{\Theta}^H\mathbf{G}_2\right) + \mathrm{tr}\left(\mathbf{\Phi}\left(\mathbf{g}_3\widehat{\mathbf{h}}_3^H\mathbf{\Theta}^H\mathbf{G}_2 + \mathbf{G}_2^H\mathbf{\Theta}\widehat{\mathbf{h}}_3\mathbf{g}_3^H\right)\right), \quad (25)$$

Thus, the objective (21a) can be expressed as in (26), shown at the bottom of the page. As for the outage constraint in (21b), unfortunately it does not admit a closed-form expression [36]. Nevertheless, it is possible to handle it by resorting to the following Bernstein-type inequality lemma to accurately approximate (21b).

Lemma 1 (Bernstein-Type Inequality: Lemma 1 in [36]): Assume $f(\mathbf{x}) = \mathbf{x}^H\mathbf{U}\mathbf{x} + 2\mathrm{Re}\{\mathbf{u}^H\mathbf{x}\} + u$, where $\mathbf{U} \in \mathbb{H}^n$, $\mathbf{u} \in \mathbb{C}^{n\times 1}$, $u \in \mathbb{R}$, and $\mathbf{x} \in \mathbb{C}^{n\times 1} \sim \mathcal{CN}(\mathbf{0}, \mathbf{I})$. Then, for any $\rho \in [0, 1]$, the following approximation holds:

$$\Pr\left\{\mathbf{x}^H\mathbf{U}\mathbf{x} + 2\mathrm{Re}\{\mathbf{u}^H\mathbf{x}\} + u \geq 0\right\} \geq 1 - \rho \quad (27a)$$

$$\Rightarrow \mathrm{Tr}\{\mathbf{U}\} - \sqrt{2\ln(1/\rho)}x + \ln(\rho)\lambda_{max}^{+}(-\mathbf{U}) + u \geq 0 \quad (27b)$$

$$\Rightarrow \begin{cases} \mathrm{Tr}\{\mathbf{U}\} - \sqrt{2\ln(1/\rho)}x + \ln(\rho)y + u \geq 0 \\ \sqrt{\|\mathbf{U}\|_F^2 + 2\|\mathbf{u}\|^2} \leq x \\ y\mathbf{I} + \mathbf{U} \succeq \mathbf{0}, y \geq 0, \end{cases} \quad (27c)$$

where x and y are slack variables, and $\mathbb{H}^n$ stands for the set of $n \times n$ complex Hermitian matrices.

In order to be able to apply Lemma 1, defining $z = \sigma_c^2(2^{C_{\mathrm{th}}} - 1)$ and $w = P_R(2^{C_{\mathrm{th}}} - 1)$, we reformulate the left-hand-side of (21b) as follows.

$$\Pr\Big((\mathbf{h}_2^H + \mathbf{h}_3^H\mathbf{\Theta}^H\mathbf{H}_1)\mathbf{t}\mathbf{t}^H(\mathbf{h}_2 + \mathbf{H}_1^H\mathbf{\Theta}\mathbf{h}_3) \geq z + w(\mathbf{g}_3^H + \mathbf{h}_3^H\mathbf{\Theta}^H\mathbf{G}_2)\mathbf{\Phi}(\mathbf{g}_3 + \mathbf{G}_2^H\mathbf{\Theta}\mathbf{h}_3)\Big) \quad (28)$$

$$= \Pr\Big(\mathbf{h}_3^H(\mathbf{\Theta}^H\mathbf{H}_1\mathbf{t}\mathbf{t}^H\mathbf{H}_1^H\mathbf{\Theta} - w\mathbf{\Theta}^H\mathbf{G}_2\mathbf{\Phi}\mathbf{G}_2^H\mathbf{\Theta})\mathbf{h}_3 + 2\Re\{(\mathbf{h}_2^H\mathbf{t}\mathbf{t}^H\mathbf{H}_1^H\mathbf{\Theta} - w\mathbf{g}_3^H\mathbf{\Phi}\mathbf{G}_2^H\mathbf{\Theta})\mathbf{h}_3\} + \mathbf{h}_2^H\mathbf{t}\mathbf{t}^H\mathbf{h}_2 - w\mathbf{g}_3^H\mathbf{\Phi}\mathbf{g}_3 - z \geq 0\Big) \quad (29)$$

$$= \Pr\Big(\Delta\mathbf{h}_3^H(\mathbf{\Theta}^H\mathbf{H}_1\mathbf{t}\mathbf{t}^H\mathbf{H}_1^H\mathbf{\Theta} - w\mathbf{\Theta}^H\mathbf{G}_2\mathbf{\Phi}\mathbf{G}_2^H\mathbf{\Theta})\Delta\mathbf{h}_3 + 2\Re\{(\mathbf{h}_2^H\mathbf{t}\mathbf{t}^H\mathbf{H}_1^H\mathbf{\Theta} - w\mathbf{g}_3^H\mathbf{\Phi}\mathbf{G}_2^H\mathbf{\Theta})\Delta\mathbf{h}_3\} + \widehat{\mathbf{h}}_3^H(\mathbf{\Theta}^H\mathbf{H}_1\mathbf{t}\mathbf{t}^H\mathbf{H}_1^H\mathbf{\Theta} - w\mathbf{\Theta}^H\mathbf{G}_2\mathbf{\Phi}\mathbf{G}_2^H\mathbf{\Theta})\widehat{\mathbf{h}}_3 + 2\Re\{(\mathbf{h}_2^H\mathbf{t}\mathbf{t}^H\mathbf{H}_1^H\mathbf{\Theta} - w\mathbf{g}_3^H\mathbf{\Phi}\mathbf{G}_2^H\mathbf{\Theta})\widehat{\mathbf{h}}_3\} + \mathbf{h}_2^H\mathbf{t}\mathbf{t}^H\mathbf{h}_2 - w\mathbf{g}_3^H\mathbf{\Phi}\mathbf{g}_3 - z \geq 0\Big). \quad (30)$$

Finally, defining

$$\mathbf{U} = \mathbf{\Theta}^H\mathbf{H}_1\mathbf{t}\mathbf{t}^H\mathbf{H}_1^H\mathbf{\Theta} - w\mathbf{\Theta}^H\mathbf{G}_2\mathbf{\Phi}\mathbf{G}_2^H\mathbf{\Theta}, \quad (31)$$

$$\mathbf{u} = \mathbf{h}_2^H\mathbf{t}\mathbf{t}^H\mathbf{H}_1^H\mathbf{\Theta} - w\mathbf{g}_3^H\mathbf{\Phi}\mathbf{G}_2^H\mathbf{\Theta}, \quad (32)$$

$$u = \widehat{\mathbf{h}}_3^H(\mathbf{\Theta}^H\mathbf{H}_1\mathbf{t}\mathbf{t}^H\mathbf{H}_1^H\mathbf{\Theta} - w\mathbf{\Theta}^H\mathbf{G}_2\mathbf{\Phi}\mathbf{G}_2^H\mathbf{\Theta})\widehat{\mathbf{h}}_3 + 2\Re\{(\mathbf{h}_2^H\mathbf{t}\mathbf{t}^H\mathbf{H}_1^H\mathbf{\Theta} - w\mathbf{g}_3^H\mathbf{\Phi}\mathbf{G}_2^H\mathbf{\Theta})\widehat{\mathbf{h}}_3\} + \mathbf{h}_2^H\mathbf{t}\mathbf{t}^H\mathbf{h}_2 - w\mathbf{g}_3^H\mathbf{\Phi}\mathbf{g}_3 - z, \quad (33)$$

the constraint in (21b) can be expressed as

$$\Pr\left(\Delta\mathbf{h}_3^H\mathbf{U}\Delta\mathbf{h}_3 + 2\Re\{\mathbf{u}^H\Delta\mathbf{h}_3\} + u \geq 0\right) \geq 1 - \rho), \quad (34)$$

which is formally equivalent to (27a), with $\Delta\mathbf{h}_3^H$ playing the role of $\mathbf{x}$. Then, we can apply Lemma 1 to reformulate (34) as

$$\mathrm{Tr}\{\mathbf{U}\} - \sqrt{2\ln(1/\rho)}x + \ln(\rho)y + u \geq 0 \quad (35)$$

$$\sqrt{\|\mathbf{U}\|_F^2 + 2\|\mathbf{u}\|^2} \leq x \quad (36)$$

$$y\mathbf{I} + \mathbf{U} \succeq \mathbf{0}, y \geq 0, \quad (37)$$

with x and y two additional slack variables.

As a result, we can reformulate Problem (21) as in Equation (38), shown at the bottom of the next page.

Similarly to the perfect CSI scenario, Problem (38) can be tackled through the alternating maximization method, iterating among the maximization of $(\mathbf{\Phi}, x, y)$, $\mathbf{\Theta}$, and $\mathbf{t}$.

Specifically, as for the optimization of the variables $(\mathbf{\Phi}, x, y)$, the objective (38a) is convex, while all constraints are linear, except for (38e), which is convex. Thus, with respect to $(\mathbf{\Phi}, x, y)$, Problem (38) can be handled by the same sequential method used for the perfect CSI case.

As for the optimization of $\mathbf{\Theta}$, Problem (38) can be handled by optimizing one RIS phase at a time, as done in the perfect CSI case.

Conversely, the optimization of $\mathbf{t}$ is somewhat more challenging, in particular due to the constraint function at the left-hand-side of (38d), which does not lead to a convex constraint and is difficult to handle by sequential convex approximations. The problem can be thus tackled by resorting to the semidefinite relaxation method. Indeed, upon defining $\mathbf{Q} = \mathbf{t}\mathbf{t}^H$, the problem with respect to $\mathbf{Q}$ can be restated as in Equation (39), shown at the bottom of the next page.

Then, by relaxing the rank-1 constraint, the problem becomes convex and thus can be solved by standard convex optimization theory. Upon obtaining the solution of the rank-relaxed version of (39), a feasible $\mathbf{t}$ can be obtained by rank reduction or randomization techniques. One approach is to use the randomized SVD technique to compute a low-rank approximation of $\mathbf{Q}$. The randomized singular value decomposition (SVD) algorithm computes an approximation of the form $\mathbf{Q} \approx \mathbf{U}_n\mathbf{\Sigma}_n\mathbf{V}_n^H$, where $\mathbf{U}_n$ and $\mathbf{V}_n$ are matrices of orthonormal columns, $\mathbf{\Sigma}_n$ is a diagonal matrix with the n largest singular values of $\mathbf{Q}$ on the diagonal, and n is the desired rank of the approximation [35]. This approximation can be obtained efficiently using random projections and can be used to compute an approximate solution for $\mathbf{t}$ as $\mathbf{t} \approx \mathbf{U}_n\mathbf{\Sigma}_n^{1/2}\mathbf{v}$,

$$\mathbb{E}[\mathrm{SINR}] = \frac{\left|\mathbf{t}^H\mathbf{h}_2\right|^2 + \mathbf{t}^H\mathbf{H}_1^H\mathbf{\Theta}\left(\widehat{\mathbf{h}}_3\widehat{\mathbf{h}}_3^H + \mathbf{\Sigma}_{h_3}\right)\mathbf{\Theta}^H\mathbf{H}_1\mathbf{t} + \mathbf{t}^H\left(\mathbf{h}_2\widehat{\mathbf{h}}_3^H\mathbf{\Theta}^H\mathbf{H}_1 + \mathbf{H}_1^H\mathbf{\Theta}\widehat{\mathbf{h}}_3\mathbf{h}_2^H\right)\mathbf{t}}{P_R L_P\left(\mathbf{g}_3^H\mathbf{\Phi}\mathbf{g}_3 + \mathrm{tr}\left(\mathbf{\Phi}\mathbf{G}_2^H\mathbf{\Theta}\left(\widehat{\mathbf{h}}_3\widehat{\mathbf{h}}_3^H + \mathbf{\Sigma}_{h_3}\right)\mathbf{\Theta}^H\mathbf{G}_2\right)\right) + \mathrm{tr}\left(\mathbf{\Phi}\left(\mathbf{g}_3\widehat{\mathbf{h}}_3^H\mathbf{\Theta}^H\mathbf{G}_2 + \mathbf{G}_2^H\mathbf{\Theta}\widehat{\mathbf{h}}_3\mathbf{g}_3^H\right)\right) + \sigma_c^2} \quad (26)$$

where $\mathbf{v}$ is a vector of appropriate size and $\mathbf{\Sigma}_n^{1/2}$ denotes the diagonal matrix with the square root of the n largest singular values of $\mathbf{Q}$ on the diagonal. Another approach is to use the randomized QR decomposition to compute a low-rank approximation of $\mathbf{t}$ [35]. The randomized QR algorithm computes an approximation of the form $\mathbf{t} \approx \mathbf{Q}_n\mathbf{c}$, where $\mathbf{Q}_n$ is a matrix of orthonormal columns and $\mathbf{c}$ is a vector of appropriate size. This approximation can be obtained efficiently using random projections and can be used to compute an approximate solution for $\mathbf{t}$. Of course, the quality of the approximation obtained using these techniques depends on the rank n of the approximation. In general, increasing n leads to a more accurate approximation, but also increases the computational cost. The optimal choice of n depends on the specific problem and the available computational resources.

V. Complexity, Convergence, and Optimality of the Proposed Solutions

In this section we analyze the complexity, convergence, and optimality of the proposed solutions under the two conditions of full CSI availability and statistical CSI availability.

A. Full CSI Case

1) Complexity: We have proposed an alternating optimization based framework for the case of full CSI that involves decoupling the three optimization variables $\mathbf{Q}_{\text{xl}}$, $\mathbf{\Phi}$, and $\mathbf{\Theta}$, and break the design optimization problem into three sub-problems. The first optimization sub-problem, given in (10), is carried out with respect to $\mathbf{Q}_{\text{xl}}$ and this sub-problem is jointly convex with respect to $\{\mathbf{Q}_{\text{xl}}\}$. Indeed, the objective and constraint functions in (10c) are linear, while the constraint in (10b) is concave. Thus, Problem (10) can be solved by means of convex optimization theory, with affordable complexity. The semidefinite matrix variable $\{\mathbf{Q}_{\text{xl}}\}$ have N^2 real scalar variables, which would result in a total complexity of $L_P\ \mathcal{O}((N^2)$ if a Lagrangian dual decomposition method is used [38]. The second optimization sub-problem, given in (11), is carried out with respect to $\mathbf{\Phi}$. The problem is relaxed into the form in (15), and a sequential method is proposed to solve it. Problem (11) is linear in $\mathbf{\Phi}$, and thus can be solved by standard interior point approaches with a complexity of $\mathcal{O}((L_PN^2)^{3.5})$. The third sub-problem is the optimization with respect to $\mathbf{\Theta}$ and we have proposed two algorithms to solve the phase shift optimization sub-problem, namely the LS based algorithm and the RP algorithm, and the two algorithms have a linear complexity in the number of RIS phase shifts, which is $\mathcal{O}(2^b \times L_R)$. Accordingly, the complexity of each iteration of the whole alternating optimization framework can be given as $(L_P\ \mathcal{O}((N^2) + \mathcal{O}((L_PN^2)^{3.5}) + \mathcal{O}(2^b \times L_R))$.

2) Convergence: It can be recognized that the objective function of (9), $\text{SINR}\left(\mathbf{\Theta}, \mathbf{Q}_{\text{xl}}, \mathbf{\Phi}\right)$, is non-decreasing during the alternating iterations of $\mathbf{\Theta}$, $\mathbf{Q}_{\text{xl}}$, and $\mathbf{\Phi}$, and is upper bounded. According to the monotone convergence theorem [39], the alternating optimization is thus guaranteed to converge in the value of the objective.

3) Optimality: The optimization problem (9) is non-convex and also mixed integer (due to the RIS discrete phase shifts). Accordingly, it is very hard to solve it achieving a globally optimal solution; however, the proposed SCA sub-algorithms are guaranteed to converge to a solution that satisfies the Karush-Kuhn-Tucker (KKT) conditions. No stronger optimality claims can be given.

B. Statistical CSI Case

1) Complexity: We first notice that all the resulting convex problems involving linear matrix inequality (LMI), second-order cone (SOC) constraints and linear constraints can be

$$\max_{\mathbf{\Phi},\mathbf{\Theta},\mathbf{t},x,y} \frac{\text{Tr}\left(\left(\mathbf{h}_2\mathbf{h}_2^H + \mathbf{H}_1^H\mathbf{\Theta}\left(\widehat{\mathbf{h}}_3\widehat{\mathbf{h}}_3^H + \mathbf{\Sigma}_{h_3}\right)\mathbf{\Theta}^H\mathbf{H}_1\right)\mathbf{t}\mathbf{t}^H + \left(\mathbf{h}_2\widehat{\mathbf{h}}_3^H\mathbf{\Theta}^H\mathbf{H}_1 + \mathbf{H}_1^H\mathbf{\Theta}\widehat{\mathbf{h}}_3\mathbf{h}_2^H\right)\mathbf{t}\mathbf{t}^H\right)}{P_RL_P\left(\mathbf{g}_3^H\mathbf{\Phi}\mathbf{g}_3 + \text{tr}\left(\mathbf{\Phi}\mathbf{G}_2^H\mathbf{\Theta}\left(\widehat{\mathbf{h}}_3\widehat{\mathbf{h}}_3^H + \mathbf{\Sigma}_{h_3}\right)\mathbf{\Theta}^H\mathbf{G}_2\right)\right) + \text{tr}\left(\mathbf{\Phi}\left(\mathbf{g}_3\widehat{\mathbf{h}}_3^H\mathbf{\Theta}^H\mathbf{G}_2 + \mathbf{G}_2^H\mathbf{\Theta}\widehat{\mathbf{h}}_3\mathbf{g}_3^H\right)\right) + \sigma_c^2} \tag{38a}$$

$$\text{Subject to: } \text{Tr}\left\{\mathbf{\Theta}^H\mathbf{H}_1\mathbf{t}\mathbf{t}^H\mathbf{H}_1^H\mathbf{\Theta} - w\mathbf{\Theta}^H\mathbf{G}_2\mathbf{\Phi}\mathbf{G}_2^H\mathbf{\Theta}\right\} - \sqrt{2\ln(1/\rho)}x + \ln(\rho)y + \widehat{\mathbf{h}}_3^H(\mathbf{\Theta}^H\mathbf{H}_1\mathbf{t}\mathbf{t}^H\mathbf{H}_1^H\mathbf{\Theta} - w\mathbf{\Theta}^H\mathbf{G}_2\mathbf{\Phi}\mathbf{G}_2^H\mathbf{\Theta})\widehat{\mathbf{h}}_3$$
$$+ 2\Re\{(\mathbf{h}_2^H\mathbf{t}\mathbf{t}^H\mathbf{H}_1^H\mathbf{\Theta} - w\mathbf{g}_3^H\mathbf{\Phi}\mathbf{G}_2^H\mathbf{\Theta})\widehat{\mathbf{h}}_3\} + \mathbf{h}_2^H\mathbf{t}\mathbf{t}^H\mathbf{h}_2 - w\mathbf{g}_3^H\mathbf{\Phi}\mathbf{g}_3 - z \geq 0 \tag{38b}$$
$$\|\mathbf{\Theta}^H\mathbf{H}_1\mathbf{t}\mathbf{t}^H\mathbf{H}_1^H\mathbf{\Theta} - w\mathbf{\Theta}^H\mathbf{G}_2\mathbf{\Phi}\mathbf{G}_2^H\mathbf{\Theta}\|_F + 2\|\mathbf{h}_2^H\mathbf{t}\mathbf{t}^H\mathbf{H}_1^H\mathbf{\Theta} - w\mathbf{g}_3^H\mathbf{\Phi}\mathbf{G}_2^H\mathbf{\Theta}\|^2 \leq x \tag{38c}$$
$$y\mathbf{I} + \mathbf{\Theta}^H\mathbf{H}_1\mathbf{t}\mathbf{t}^H\mathbf{H}_1^H\mathbf{\Theta} - w\mathbf{\Theta}^H\mathbf{G}_2\mathbf{\Phi}\mathbf{G}_2^H\mathbf{\Theta} \succeq \mathbf{0}, y \geq 0 \tag{38d}$$
$$L_P\|\mathbf{t}\|^2 \leq P_C,\ (9d),\ (9e) \tag{38e}$$

$$\max_{\mathbf{Q}} \text{Tr}\left(\left(\mathbf{h}_2\mathbf{h}_2^H + \mathbf{H}_1^H\mathbf{\Theta}\left(\widehat{\mathbf{h}}_3\widehat{\mathbf{h}}_3^H + \mathbf{\Sigma}_{h_3}\right)\mathbf{\Theta}^H\mathbf{H}_1\right)\mathbf{Q} + \left(\mathbf{h}_2\widehat{\mathbf{h}}_3^H\mathbf{\Theta}^H\mathbf{H}_1 + \mathbf{H}_1\mathbf{\Theta}\widehat{\mathbf{h}}_3\mathbf{h}_2^H\right)\mathbf{Q}\right) \tag{39a}$$

$$\text{Subject to: } \text{Tr}\left\{\mathbf{\Theta}^H\mathbf{H}_1\mathbf{Q}\mathbf{H}_1^H\mathbf{\Theta} - w\mathbf{\Theta}^H\mathbf{G}_2\mathbf{\Phi}\mathbf{G}_2^H\mathbf{\Theta}\right\} - \sqrt{2\ln(1/\rho)}x + \ln(\rho)y + \widehat{\mathbf{h}}_3^H(\mathbf{\Theta}^H\mathbf{H}_1\mathbf{Q}\mathbf{H}_1^H\mathbf{\Theta} - w\mathbf{\Theta}^H\mathbf{G}_2\mathbf{\Phi}\mathbf{G}_2^H\mathbf{\Theta})\widehat{\mathbf{h}}_3$$
$$+ 2\Re\{(\mathbf{h}_2^H\mathbf{Q}\mathbf{H}_1^H\mathbf{\Theta} - w\mathbf{g}_3^H\mathbf{\Phi}\mathbf{G}_2^H\mathbf{\Theta})\widehat{\mathbf{h}}_3\} + \mathbf{h}_2^H\mathbf{Q}\mathbf{h}_2 - w\mathbf{g}_3^H\mathbf{\Phi}\mathbf{g}_3 - z \geq 0 \tag{39b}$$
$$\|\mathbf{\Theta}^H\mathbf{H}_1\mathbf{Q}\mathbf{H}_1^H\mathbf{\Theta} - w\mathbf{\Theta}^H\mathbf{G}_2\mathbf{\Phi}\mathbf{G}_2^H\mathbf{\Theta}\|_F + 2\|\mathbf{h}_2^H\mathbf{Q}\mathbf{H}_1^H\mathbf{\Theta} - w\mathbf{g}_3^H\mathbf{\Phi}\mathbf{G}_2^H\mathbf{\Theta}\|^2 \leq x \tag{39c}$$
$$y\mathbf{I} + \mathbf{\Theta}^H\mathbf{H}_1\mathbf{Q}\mathbf{H}_1^H\mathbf{\Theta} - w\mathbf{\Theta}^H\mathbf{G}_2\mathbf{\Phi}\mathbf{G}_2^H\mathbf{\Theta} \succeq \mathbf{0}, y \geq 0 \tag{39d}$$
$$L_P\text{Tr}(\mathbf{Q}) \leq P_C,\ \text{rank}(\mathbf{Q}) = 1,\ (9d),\ (9e) \tag{39e}$$

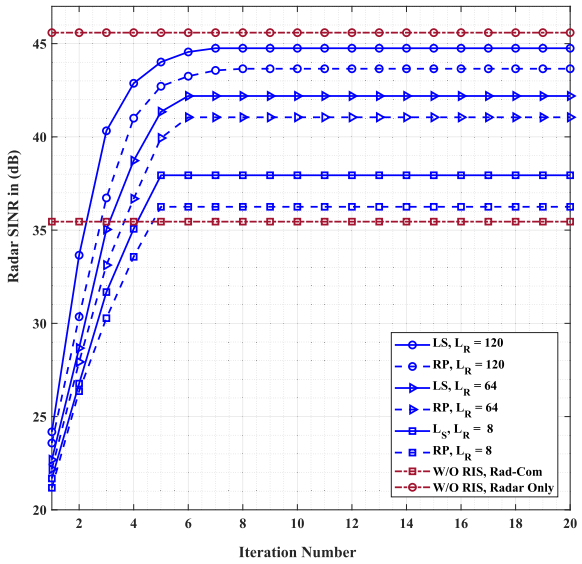

Fig. 3. The convergence behavior of the proposed framework with either linear search and relaxations and projection phase shift optimization algorithms at $\gamma = 10$dB, and $N = 16$.

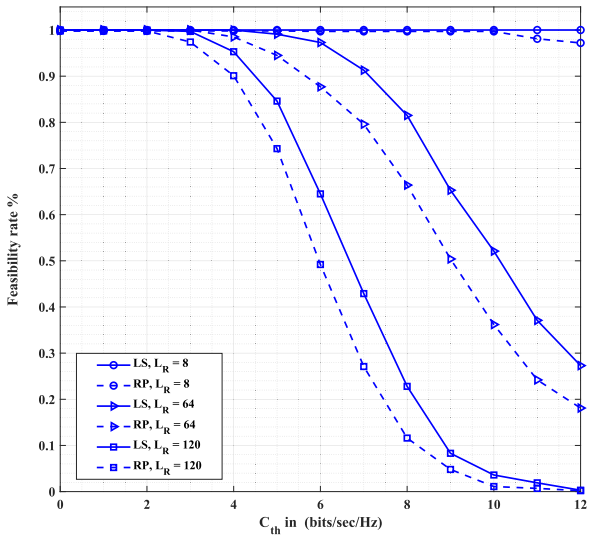

Fig. 4. Feasibility rate versus the communication outage threshold level for the proposed RIS-assisted framework with either LS and LS, with $N = 16$, $\gamma = 10$ dB.

solved by a standard interior point algorithms. The computational complexity of the statistical CSI scenario design in terms of the worst-case run-time, can be thus expressed as [40]:

$$\mathcal{O}((\sum_{j=1}^{J} b_j + 2I)^{1/2} n(n^2 + \underbrace{n\sum_{j=1}^{J} b_j^2 + \sum_{j=1}^{J} b_j^3}_{\text{due to LMI}} + \underbrace{n\sum_{i=1}^{I} a_i^2}_{\text{due to SOC}}))$$

where n is the number of variables, J is the number of LMIs of size b_j, and I is the number of SOC of size a_i. Based on the above expression, the approximate computational complexity per iteration for problems (42) and (43), according to the following reference, are:

$$O_{\mathbf{\Phi}} = \mathcal{O}([2(M_t+1)]^{1/2} M_t [M_t^2 + 2M_t^3 + 2M_t^4 + M^3(M_t+1)^2])$$
$$O_{\mathbf{Q}} = \mathcal{O}([4M_t+2N]^{1/2} N [N^2 + N(M_t(N^2 + (M_t+1)^2) + N)]),$$

respectively. Accordingly, the whole complexity equals $O_{\mathbf{\Phi}} + O_{\mathbf{Q}} + 2^b \times L_R$.

2) Convergence: By employing a similar methodology applied in the case of full CSI, it becomes evident that the objective function associated with the statistical CSI scenario, shown in (38) and (39), exhibits a non-decreasing trend throughout the alternating iterations involving variables $\mathbf{\Theta}$, $\mathbf{Q}_{\text{xl}}$, and $\mathbf{\Phi}$. Additionally, it is observed that the objective function remains bounded from above. Consequently, applying the monotone convergence theorem [39], we can assert that the alternating optimization process is guaranteed to converge in the value of the objective.

3) Optimality: Once again, it is very hard and still an open problem to obtain a globally optimal solution to the problem in (38) and (39). However, the proposed suboptimal solution is guaranteed to converge to a point that satisfies the KKT conditions. No stronger optimality claims can be given.

VI. Simulation Results

In this section, we provide simulation results to evaluate the performance of the proposed RIS-assisted spectrum sharing approaches for optimized communication-radar coexistence. The used numerical values for the system parameters are listed in Table I. Based on such values, the possible signal-to-noise (SNR) range at the communication receiver is between 12 dB and 30 dB, which is supported by LTE systems [37]. On the other hand, the required SNR per single antenna, for a typical radar system operating with probability of detection of 0.9 and probability of false alarm of 10^{-6}, equals about 13.2 dB [33]. However, the actual SNR may be much smaller than these values due to the use of some DoFs to mitigate the interference generated by the communication system. The simulated system setup for both the perfect and imperfect CSI scenarios is organized such that the communication BS, the RIS, and the radar are installed at $(0, 0)$, $(110, 50)$, and $(200, 0)$, respectively, with the location of user chosen at each iteration as a point inside a user circle centered at $(110, 25)$.

A. Perfect Channel Scenario

In this section, we analyze the proposed RIS-aided spectrum sharing approach under the assumption of perfect CSI. We will first analyze the convergence rate and feasibility of the proposed approach. Next, we will show the effect of some system parameters on the performance of the system.

Fig. 3 provides the convergence behavior of the proposed framework versus the iteration number of the outer loop, with perfect CSI availability and with either linear search, expressed as **LS** in the legend, and relaxation and projection, expressed as **RP** in the legend. Here, the outage capacity threshold for the communication user is set to $C_{\text{th}} = 3$ bits/sec/Hz, and the ratio between radar and communication power budgets, namely γ, is set to 10 dB. We have tested the convergence of our proposed solution with three values of the number of RIS

TABLE I
SIMULATION PARAMETERS

Parameters	Values
Radar antenna numbers (N)	16
Commun. Tx antennas (M_t)	8
Commun. Rx antennas (M_r)	8
Inter-element spacing (d)	$\lambda_c/2$
Direct channel PL (D) in dB	$32.6 + 36.7\log_{10}(D)$
Indirect channel PL (D) in dB	$35.6 + 22\log_{10}(D)$
Number of targets (K)	3
Rician factor for ($\mathcal{K}$)	8
Directions of targets (ϕ_k)	$0°, 15°, 30°$
The constant ζ in (15c)	0.9
Length of radar waveform (L_P)	16 pulses
Commun. power budget (P_C)	6400 wrt thermal noise
Radar power budget (P_R)	$1000 \times P_C$
AWGN variances (σ_C^2,σ_R^2)	(1,1)
Number of discrete angle levels	8

reflective elements, $L_R = 8, 64,$ and 120. Additionally, the proposed framework is compared with two benchmark scenarios. The first benchmark scenario is the radar-communication coexistence scenario without RIS, named "W/O RIS, Rad-Com" in the legend, while the second benchmark scenario is the radar only scenario without RIS, named "W/O" RIS, Radar Only" in the legend. It is apparent that the proposed framework converges faster with a smaller number of RIS elements. Additionally, the proposed framework with any number of RIS reflective elements provides a better performance compared with the case of Rad-communication coexistence without RIS, due to the interference provided at radar receiver by the communication transmitter. This also illustrates the importance of RIS in mitigating the mutual interference between the two systems. The "radar only without RIS" scenario represents the upper bound for our proposed framework, since it corresponds to the case in which there is no interference suffered at radar receiver. It is obvious from Fig. 3 that the higher the number of RIS elements, the better will be the radar SINR, due to the larger diversity gain provided with higher number of reflective elements.

In order to prove the effect of the communication system transmissions on the radar system performance, we study the feasibility of the proposed framework with different communication outage threshold (C_{th}) level. The feasibility rate is defined as the ratio of the number of feasible[1] channel realizations to the total number of channel realizations. Fig. 4 shows the feasibility rate versus the communication outage threshold level (C_{th}) for the proposed RIS-assisted framework with either linear search or relaxation and projection phase optimization algorithms for different values of RIS elements. Generally, the proposed framework has slightly larger feasibility rate when the linear search phase shift optimization method is employed, compared to the case of in which the relaxation and projection method is used. Additionally, the feasibility rate decreases as the outage threshold (C_{th}) increases. With smaller number of RIS elements, the communication outage constraint

[1]We mean by feasible channel realization, the realization with which there exists a feasible solution to the outage constrained problem in (9).

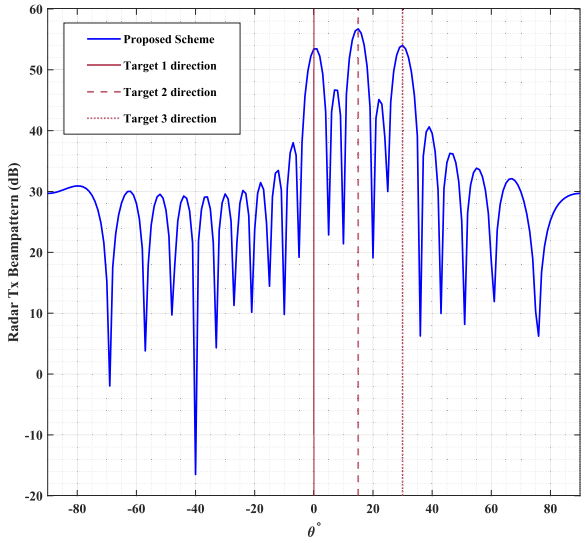

Fig. 5. The Beampattern for the proposed algorithm.

is almost guaranteed to be met till $C_{\text{th}} = 10$ bits/sec/Hz, and accordingly, the feasibility rate is almost equal to one. However, it seems that a larger number of RIS elements provides more degrees-of-freedom for optimizing the phase shifts that satisfy the constraints of the problem. But, it is noticed that increasing the number of RIS elements will also lead to increasing the size of the covariance matrix of the radar. This, in turn, fortifies the trade-off between the two systems metrics, limits the solution space and accordingly leads to a decrease of the feasibility rate.

Fig. 5 shows the radar beampattern designed by our proposed framework. It is worth noting that the main lobes of the proposed approach are aligned toward the three targets that are assumed to be at angles $0°, 15°,$ and $30°$, which indicates that our proposed radar beamforming design has good directivity properties toward the targets directions, and the side lobes are below the mainlobes by about 20 dB. Accordingly, our design has better ability to suppress the communication interference from the radar receiver.

Fig. 6 shows the effect of the number of the RIS elements and of the radar to communication power budget ratio (γ) on the radar SINR. First of all, increasing γ leads to an analogous increase in the radar SINR: this behavior is intuitive as both the increase in radar power and the decrease in communication power will lead to the increase in radar SINR. Additionally, the LS phase shift optimization algorithms helps in achieving a slight increase in radar SINR compared with the relaxation and projection algorithm. Moreover, uniformly with respect to the power ratio, the increase in the number of RIS reflective elements leads to an increase in radar SINR, since the RIS helps to mitigate the interference while providing diversity. Specifically, increasing the number of RIS elements (L_R) by 100 elements leads to increasing the radar SINR by 4 dB with both the linear search and the projection gradient algorithms.

Using the Neyman-Pearson criterion, the MIMO radar's asymptotic target detection probability, P_D, can be assessed, under the assumption of Gaussian-distributed interference,

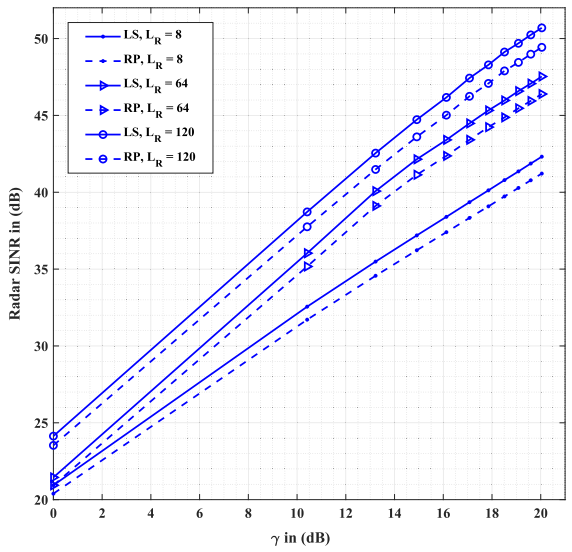

Fig. 6. Radar SINR versus the radar to communication powers ratio for the proposed RIS-assisted framework.

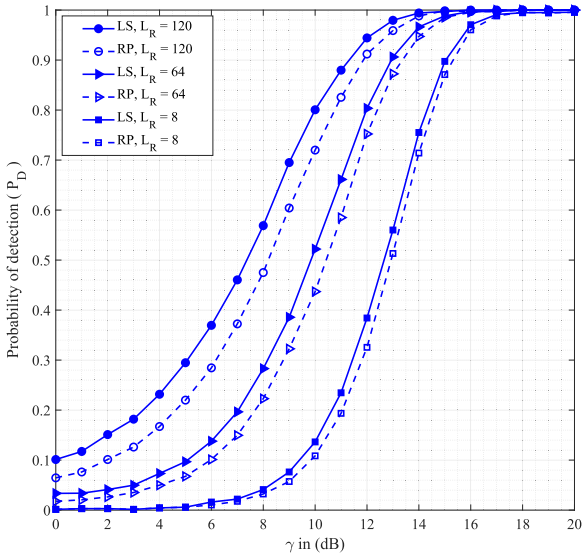

Fig. 7. Radar probability of detection (P_D) versus the radar to communication powers ratio for the proposed RIS-assisted framework, with probability of false alarm $P_{FA} = 10^{-4}$.

utilizing the generalized likelihood ratio test (GLRT) [31]:

$$P_D = 1 - \varphi_{\chi^2_2(\nu))} \left(\varphi^{-1}_{\chi^2_2(\nu))}(1 - P_{FA}) \right)$$

where P_{FA} is the probability of false alarm, the functions $\varphi_{\chi^2_2(\nu))}$ and $\varphi^{-1}_{\chi^2_2(\nu))}$ refer to the non-central chi-square cumulative distribution function (CDF) with 2 degrees-of-freedoms (DoFs) and its inverse function, respectively, and ν is the non-centrality parameters for $\varphi_{\chi^2_2(\nu))}$, and it is expressed as:

$$\nu = L_P N \ \ \mathrm{tr}\left(\frac{\mathbf{\Phi} \mathbf{D}_t}{\mathbf{G}_{\text{eff}} \ \mathbf{Q}_{\text{xl}} \ \mathbf{G}^H_{\text{eff}} + \sigma^2_R} \right) .$$

In the above expression, we recall that $\mathbf{D}_t = \sum_k \sigma^2_{\beta_k} \mathbf{v}^*_t(\phi_k) \, \mathbf{v}^T_t(\phi_k)$, $\mathbf{Q}_{\text{xl}}$ denotes the interference covariance matrix of the radar sensing waveform for all $l \in \mathbb{N}^+_{L_P}$, $\mathbf{G}_{\text{eff}} = \mathbf{G}^H_1 + \mathbf{G}^H_2 \mathbf{\Theta}^H \mathbf{H}_1$ and $\mathbf{F}\mathbf{F}^H = L_P \mathbf{\Phi}$.

It is important to emphasize that the above expression of P_D of the MIMO radar is applicable only to scenarios where white Gaussian noise is present [31], [32]. Assuming that the resulting interference-plus-noise signal remains Gaussian distributed with zero mean, but with a non-identity covariance matrix, a whitening filter can be employed in our design, ensuring that the derivation in [31] remains applicable to our proposed model. Figure 7 illustrates the variation of P_D versus the radar to communication powers ratio for the proposed RIS-assisted spectrum sharing framework at a probability of false alarm, P_{FA}, equal to 10^{-4}. It is well known that P_D is an increasing function of the radar signal-to-interference-plus-noise ratio (SINR). Therefore, the variation of P_D versus γ shown above is analogous to the variation of the SINR versus γ shown in Fig. 6.

B. Imperfect Channel Scenario

We now study the performance of the proposed robust RIS-aided spectrum sharing scenario described in Section IV. The proposed framework under statistical error model with

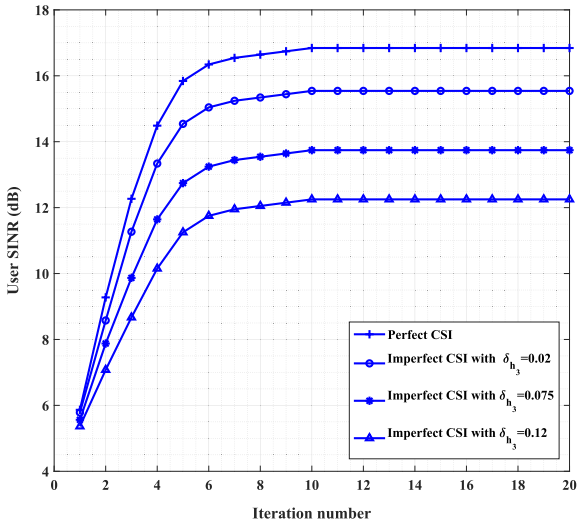

Fig. 8. The convergence behavior of the proposed robust framework at $\gamma = 10$ dB, $N = 16$, and $C_{\text{th}} = 8$ bits/Sec/Hz.

CSI uncertainty are labeled in the legend as "Imperfect CSI" accompanied with the uncertainty level $\delta_{\mathbf{h}_3}$. For the statistical CSI error model, the variance of $\mathbf{h}_3$ is defined as $\delta^2_{\mathbf{h}_3} \|\widehat{\mathbf{h}}_3\|^2_2$. It is worth noting that $\delta_{\mathbf{h}_3} \in [0, 1)$ specifies the level of CSI uncertainties in the RIS-to-user channel $\mathbf{h}_3$.

Fig. 8 provides the convergence behavior of the proposed robust RIS-assisted design framework. In this scenario, we set the communication outage threshold as $C_{\text{th}} = 8$ bits/sec/Hz, and the CSI uncertainty for the RIS-to-user channel as $\{\delta_{\mathbf{h}_3} = 0.03$. It can be seen that all the proposed frameworks converge within the first 8 outer iterations. It is worth noting that the proposed framework converges to larger user SINR levels as the uncertainty level implied by $\delta_{\mathbf{h}_3}$ decreases. It is also of great importance to note that the proposed robust framework

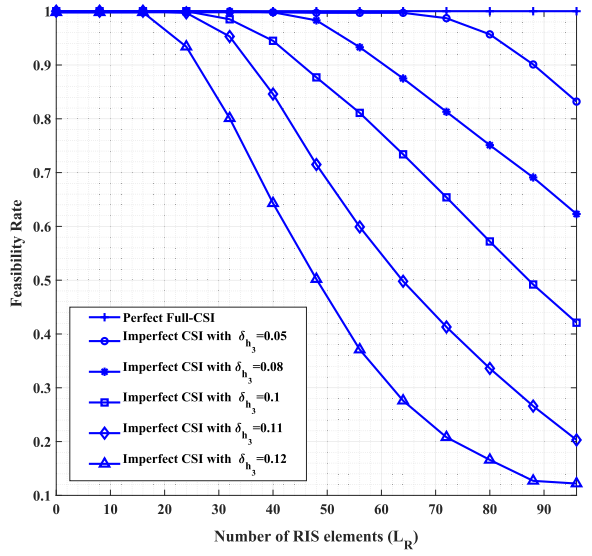

Fig. 9. Feasibility rate versus the number of RIS elements for the proposed robust RIS-assisted framework at different uncertainty levels, with $N = 16$, $\gamma = 10$ dB, and $C_{\rm th} = 8$ bits/sec/Hz.

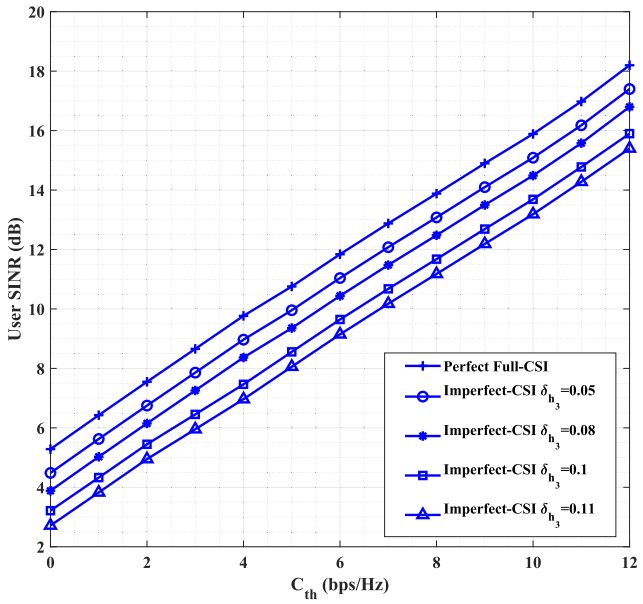

Fig. 10. Received user SINR with statistical CSI uncertainty versus the communication outage threshold rate $C_{\rm th}$, $N = 16$, $\gamma = 10$ dB, $L_R = 64$.

converges approximately within the same number of iterations as in the perfect full-CSI scenarios.

In Fig. 9, we study the feasibility of the proposed framework with different number of RIS elements (L_R) in terms of the feasibility rate. Fig. 9 shows the feasibility rate versus the number of RIS elements (L_R) for the proposed robust RIS-assisted framework while assuming different accuracy levels for the CSI of channel $\mathbf{h}_3$. It is worth mentioning that the accuracy becomes 100% when the uncertainty parameter $\delta_{\mathbf{h}_3}$ equals zero. Generally, the feasibility rate decreases as the CSI uncertainty of channel $\mathbf{h}_3$ increases. With perfect CSI of $\mathbf{h}_3$, the communication outage constraint is almost guaranteed to be met, and accordingly, the feasibility rate is almost equal one, while with CSI uncertainty, the feasibility rate decreases as the uncertainty level increases. Additionally, the feasibility of the design problem decreases as the number of RIS elements increases.

Fig. 10 shows the effect of the communication outage threshold level $C_{\rm th}$ on the performance of the proposed robust RIS-assisted framework at different uncertainty levels. Generally, the received user SINR increases as the communication outage threshold level increases at any number of RIS elements. This is due to the fact that the radar and communication systems are sharing the same spectrum band and introduce interference to one another. So, the increase in $C_{\rm th}$ implies an increase in the communication power. It is seen in Fig. 10 that the framework based on the statistical CSI error model provides a slightly lower users' SINR compared to the case with perfect $\mathbf{h}_3$ CSI. Thus, the proposed statistical framework is quite robust to the lack of perfect CSI of the channel $\mathbf{h}_3$. Also, as expected, the received user SINR is generally decreasing as the CSI uncertainty increases.

In Fig. 11, the received SINR achieved by the communication user while employing statistical CSI uncertainty for $\mathbf{h}_3$, is plotted versus the number of RIS elements for different

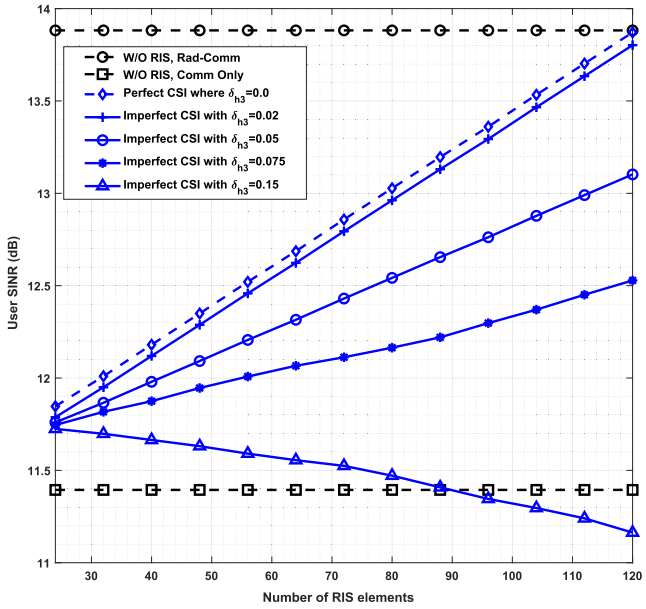

Fig. 11. Received user SINR with statistical CSI uncertainty versus the number of RIS elements at different levels of CSI accuracy, $N = 16$, $P_C = P_R$.

levels of channel uncertainty. It is seen from Fig. 11 that, except for $\delta_{\mathbf{h}_3} = 0.15$, the received SINR of the communication user increases by increasing the number of RIS elements. However, the rate increases slowlier as the uncertainty parameter $\delta_{\mathbf{h}_3}$ increases. However, as the uncertainty parameter increases to 0.15, the received SINR of the communication user begins to decrease when the number of RIS elements increases. In other words, the received SINR at the user decreases as the uncertainty parameter $\delta_{\mathbf{h}_3}$ increases due to the larger power required by the communication system to fulfill

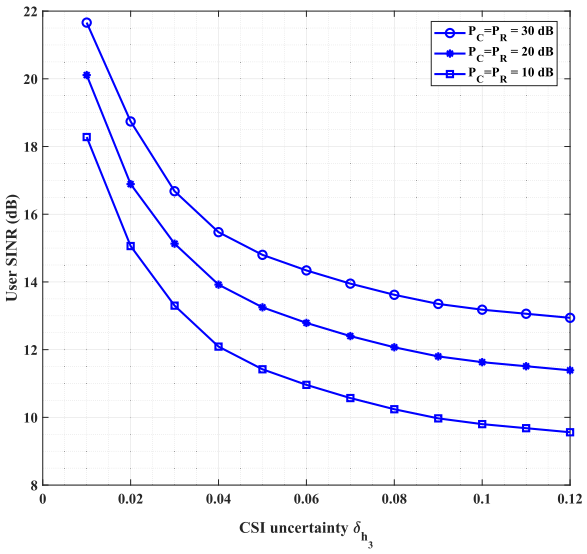

Fig. 12. Received SINR at the communication user under statistical CSI uncertainty versus the uncertainty parameter $\delta_{\mathbf{h}_3}$ at different communication power budgets, $N = 16$, $P_C = P_R$, $L_R = 64$.

the outage constraint due to the lower CSI accuracy. In turn, this increases the received SINR at the user receiver. Here, two benchmark scenarios have been shown for the case of no RIS. The case labeled with No RIS Rad-Com represents the lower bound where the radar system suffers interference from the communication system and there is no RIS to improve the diversity gain, and, consequently, the radar SINR. The other benchmark considers the case of communication only with no RIS deployment, so the received SINR at user receiver does not suffer any interference. This case represents an upper bound for the user SINR. Finally, Fig. 12 shows the effect of the uncertainty parameter $\delta_{\mathbf{h}_3}$ on the received SINR at the communication user. At any level of communication power budget, the received SINR at the communication user receiver decreases as the uncertainty parameter increases, which coincides with the conclusions from previous numerical results.

VII. Conclusion

In this paper, we employed RIS to improve coexistence between radar and communication systems through exploiting the RIS capability to manipulate the propagation environment. Under the assumption of perfect CSI, we investigated how to jointly design the communication transmit covariance, the passive beamforming of the RIS, and the active beamforming at the radar system. The radar output SINR was maximized subject to the constraints of radar and communication power budgets, communication rate outage or QoS, and RIS coefficients. We also extended the proposed algorithm by developing a robust RIS-aided radar communication framework while considering a statistical CSI error model for the RIS-user channel. The results have shown that employing a RIS in a radar communication coexistence scenario can greatly improve the communication performance while ensuring satisfactory radar performance. Moreover, it has been shown that, if not accounted for by a proper design, the channel uncertainty can limit the improvement provided by the RIS.

References

[1] F. Liu et al., "Integrated sensing and communications: Toward dual-functional wireless networks for 6G and beyond," *IEEE J. Sel. Areas Commun.*, vol. 40, no. 6, pp. 1728–1767, Jun. 2022.

[2] J. A. Zhang et al., "Enabling joint communication and radar sensing in mobile networks—A survey," *IEEE Commun. Surveys Tuts.*, vol. 24, no. 1, pp. 306–345, 1st Quart., 2022.

[3] A. Khawar, A. Abdelhadi, and C. Clancy, "Target detection performance of spectrum sharing MIMO radars," *IEEE Sensors J.*, vol. 15, no. 9, pp. 4928–4940, Sep. 2015.

[4] J. A. Mahal, A. Khawar, A. Abdelhadi, and T. C. Clancy, "Spectral coexistence of MIMO radar and MIMO cellular system," *IEEE Trans. Aerosp. Electron. Syst.*, vol. 53, no. 2, pp. 655–668, Apr. 2017.

[5] F. Liu, C. Masouros, A. Li, T. Ratnarajah, and J. Zhou, "MIMO radar and cellular coexistence: A power-efficient approach enabled by interference exploitation," *IEEE Trans. Signal Process.*, vol. 66, no. 14, pp. 3681–3695, Jul. 2018.

[6] F. Liu, C. Masouros, A. Li, and T. Ratnarajah, "Robust MIMO beamforming for cellular and radar coexistence," *IEEE Wireless Commun. Lett.*, vol. 6, no. 3, pp. 374–377, Jun. 2017.

[7] M. Di Renzo et al., "Smart radio environments empowered by reconfigurable intelligent surfaces: How it works, state of research, and the road ahead," *IEEE J. Sel. Areas Commun.*, vol. 38, no. 11, pp. 2450–2525, Nov. 2020.

[8] X. Wang, Z. Fei, J. Guo, Z. Zheng, and B. Li, "RIS-assisted spectrum sharing between MIMO radar and MU-MISO communication systems," *IEEE Wireless Commun. Lett.*, vol. 10, no. 3, pp. 594–598, Mar. 2021.

[9] X. Wang, Z. Fei, Z. Zheng, and J. Guo, "Joint waveform design and passive beamforming for RIS-assisted dual-functional radar-communication system," *IEEE Trans. Veh. Technol.*, vol. 70, no. 5, pp. 5131–5136, May 2021.

[10] Y. He, Y. Cai, H. Mao, and G. Yu, "RIS-assisted communication radar coexistence: Joint beamforming design and analysis," *IEEE J. Sel. Areas Commun.*, vol. 40, no. 7, pp. 2131–2145, Jul. 2022.

[11] Q. Wu, S. Zhang, B. Zheng, C. You, and R. Zhang, "Intelligent reflecting surface-aided wireless communications: A tutorial," *IEEE Trans. Commun.*, vol. 69, no. 5, pp. 3313–3351, May 2021.

[12] W. Tang et al., "Wireless communications with programmable metasurface: New paradigms, opportunities, and challenges on transceiver design," *IEEE Wireless Commun.*, vol. 27, no. 2, pp. 180–187, Apr. 2020.

[13] X. Ma, S. Guo, H. Zhang, Y. Fang, and D. Yuan, "Joint beamforming and reflecting design in reconfigurable intelligent surface-aided multi-user communication systems," *IEEE Trans. Wireless Commun.*, vol. 20, no. 5, pp. 3269–3283, May 2021.

[14] S. Buzzi, E. Grossi, M. Lops, and L. Venturino, "Radar target detection aided by reconfigurable intelligent surfaces," *IEEE Signal Process. Lett.*, vol. 28, pp. 1315–1319, 2021.

[15] Z.-M. Jiang et al., "Intelligent reflecting surface aided dual-function radar and communication system," *IEEE Syst. J.*, vol. 16, no. 1, pp. 475–486, Mar. 2022.

[16] S. P. Chepuri, N. Shlezinger, F. Liu, G. C. Alexandropoulos, S. Buzzi, and Y. C. Eldar, "Integrated sensing and communications with reconfigurable intelligent surfaces," 2022, *arXiv:2211.01003*.

[17] F. Wang, H. Li, and M. A. Govoni, "Power allocation and co-design of multicarrier communication and radar systems for spectral coexistence," *IEEE Trans. Signal Process.*, vol. 67, no. 14, pp. 3818–3831, Jul. 2019.

[18] B. Hong, W.-Q. Wang, and C.-C. Liu, "Interference utilization for spectrum sharing radar-communication systems," *IEEE Trans. Veh. Technol.*, vol. 70, no. 8, pp. 8304–8308, Aug. 2021.

[19] M. Rihan and L. Huang, "Optimum co-design of spectrum sharing between MIMO radar and MIMO communication systems: An interference alignment approach," *IEEE Trans. Veh. Technol.*, vol. 67, no. 12, pp. 11667–11680, Dec. 2018.

[20] P. Xu, G. Chen, G. Pan, and M. D. Renzo, "Ergodic secrecy rate of RIS-assisted communication systems in the presence of discrete phase shifts and multiple eavesdroppers," *IEEE Wireless Commun. Lett.*, vol. 10, no. 3, pp. 629–633, Mar. 2021.

[21] C. Huang, A. Zappone, G. C. Alexandropoulos, M. Debbah, and C. Yuen, "Reconfigurable intelligent surfaces for energy efficiency in wireless communication," *IEEE Trans. Wireless Commun.*, vol. 18, no. 8, pp. 4157–4170, Aug. 2019.

[22] Z. Yu, X. Hu, C. Liu, M. Peng, and C. Zhong, "Location sensing and beamforming design for IRS-enabled multi-user ISAC systems," *IEEE Trans. Signal Process.*, vol. 70, pp. 5178–5193, 2022.

[23] X. Hu, C. Liu, M. Peng, and C. Zhong, "IRS-based integrated location sensing and communication for mmWave SIMO systems," *IEEE Trans. Wireless Commun.*, vol. 22, no. 6, pp. 4132–4145, Jun. 2023.

[24] L. You, J. Xiong, D. W. K. Ng, C. Yuen, W. Wang, and X. Gao, "Energy efficiency and spectral efficiency tradeoff in RIS-aided multiuser MIMO uplink transmission," *IEEE Trans. Signal Process.*, vol. 69, pp. 1407–1421, 2021.

[25] C. Wang, J. Tong, G. Cui, X. Zhao, and W. Wang, "Robust interference cancellation for vehicular communication and radar coexistence," *IEEE Commun. Lett.*, vol. 24, no. 10, pp. 2367–2370, Oct. 2020.

[26] N. Su, F. Liu, and C. Masouros, "Secure radar-communication systems with malicious targets: Integrating radar, communications and jamming functionalities," *IEEE Trans. Wireless Commun.*, vol. 20, no. 1, pp. 83–95, Jan. 2021.

[27] P. Liu, Z. Fei, X. Wang, B. Li, Y. Huang, and Z. Zhang, "Outage constrained robust secure beamforming in integrated sensing and communication systems," *IEEE Wireless Commun. Lett.*, vol. 11, no. 11, pp. 2260–2264, Nov. 2022.

[28] D. Xu, X. Yu, D. W. K. Ng, A. Schmeink, and R. Schober, "Robust and secure resource allocation for ISAC systems: A novel optimization framework for variable-length snapshots," *IEEE Trans. Commun.*, vol. 70, no. 12, pp. 8196–8214, Dec. 2022.

[29] S. Abeywickrama, R. Zhang, Q. Wu, and C. Yuen, "Intelligent reflecting surface: Practical phase shift model and beamforming optimization," *IEEE Trans. Commun.*, vol. 68, no. 9, pp. 5849–5863, Sep. 2020.

[30] B. Li and A. P. Petropulu, "Joint transmit designs for coexistence of MIMO wireless communications and sparse sensing radars in clutter," *IEEE Trans. Aerosp. Electron. Syst.*, vol. 53, no. 6, pp. 2846–2864, Dec. 2017.

[31] S. M. Kay, *Fundamentals of Statistical Signal Processing, Volume II: Detection Theory*, vol. 2. Upper Saddle River, NJ, USA: Prentice-Hall, 1998.

[32] I. Bekkerman and J. Tabrikian, "Target detection and localization using MIMO radars and sonars," *IEEE Trans. Signal Process.*, vol. 54, no. 10, pp. 3873–3883, Oct. 2006.

[33] B. Li, A. P. Petropulu, and W. Trappe, "Optimum co-design for spectrum sharing between matrix completion based MIMO radars and a MIMO communication system," *IEEE Trans. Signal Process.*, vol. 64, no. 17, pp. 4562–4575, Sep. 2016.

[34] Z. Wang, L. Liu, and S. Cui, "Channel estimation for intelligent reflecting surface assisted multiuser communications: Framework, algorithms, and analysis," *IEEE Trans. Wireless Commun.*, vol. 19, no. 10, pp. 6607–6620, Oct. 2020.

[35] G. Strang, *Linear Algebra and Its Applications*. Belmont, CA, USA: Thomson, Brooks/Cole, 2006.

[36] K.-Y. Wang, A. M. So, T.-H. Chang, W.-K. Ma, and C.-Y. Chi, "Outage constrained robust transmit optimization for multiuser MISO downlinks: Tractable approximations by conic optimization," *IEEE Trans. Signal Process.*, vol. 62, no. 21, pp. 5690–5705, Nov. 2014.

[37] *LTE; Evolved Universal Terrestrial Radio Access (E-UTRA) Physical Layer Procedures*, document TS 36.213, V8.0, 3GPP, 2009.

[38] S. Boyd and L. Vandenberghe, *Convex Optimization*. Cambridge, U.K.: Cambridge Univ. Press, 2004.

[39] J. Yeh, *Real Analysis: Theory of Measure and Integration*, 2nd ed. Singapore: World Scientific, 2006.

[40] A. Ben-Tal and A. Nemirovski, *Lectures on Modern Convex Optimization: Analysis, Algorithms, and Engineering Applications*. Philadelphia, PA, USA: SIAM, 2001.

Mohamed Rihan (Senior Member, IEEE) received the B.Sc. degree (Hons.) from Menoufia University, Menouf, Egypt, in 2005, and the M.Sc. and Ph.D. degrees in electronics and communication engineering from the Egypt–Japan University of Science and Technology, New Borg El Arab, Egypt, in 2012 and 2015, respectively. During his academic journey, he displayed a keen interest in cutting-edge research and collaborated with prestigious institutions worldwide. From 2014 to 2015, he was a Researcher with the Department of Advanced Information Technology, Graduate School of ISEE, Kyushu University, Fukuoka, Japan. He was an Adjunct Professor with the Center of Photonics and Smart Materials, Zewail City of Science and Technology, Giza, Egypt, from 2016 to 2017. From 2017 to 2021, he was an Associate Researcher with the College of Information Engineering, Shenzhen University, Shenzhen, China, where he expertise in the field of integrated radar sensing and communication, signal processing applications, and integrated terrestrial and non-terrestrial (NTN) networks. Currently, he is a Marie Curie Research Fellow with the Department of Electrical and Information Engineering, University of Cassino and Southern Lazio, Cassino, Italy. He is also an Associate Professor with the Faculty of Electronic Engineering, Menoufia University. His dedication to academia and research has led to numerous contributions and breakthroughs in the field of wireless communications. His current research interests include integrated radar sensing and communication, signal processing applications, integrated terrestrial and non-terrestrial (NTN) networks, and the integration of artificial intelligence into wireless communications.

Alessio Zappone (Senior Member, IEEE) received the M.Sc. and Ph.D. degrees from the University of Cassino and Southern Lazio, Cassino, Italy.

From 2012 to 2016, he was with the Dresden University of Technology, where he is managing the Project "CEMRIN on energy-efficient resource allocation in wireless networks" funded by the German Research Foundation (DFG). Since 2019, he has been a Professor with the University of Cassino and Southern Lazio. His current research interests include communication theory and signal processing, with a main focus on optimization techniques for resource allocation and energy efficiency maximization. In 2017, he was a recipient of the H2020 Marie Curie IF BESMART Fellowship for experienced researchers carried out at the LANEAS Group of CentraleSupelec, Gif-sur-Yvette, France. For his research, he received the 2021 Marconi Award and the 2023 Fred Ellersick Award from the IEEE Communications Society. He serves as a Senior Area Editor for the IEEE SIGNAL PROCESSING LETTERS, an Editor for the IEEE TRANSACTIONS ON WIRELESS COMMUNICATIONS and IEEE COMMUNICATIONS LETTERS, and a Guest Editor for the IEEE JOURNAL ON SELECTED AREAS ON COMMUNICATIONS.

Stefano Buzzi (Senior Member, IEEE) received the M.Sc. degree (summa cum laude) in electronic engineering and the Ph.D. degree in electrical and computer engineering from the University of Naples Federico II in 1994 and 1999, respectively.

He has had short-term research appointments at Princeton University, Princeton, NJ, USA, in 1999, 2000, 2001, and 2006. He joined as an Assistant Professor with the University of Cassino and Lazio Meridionale, Italy, in 2000, where he has been an Associate Professor since 2002 and has been a Full Professor since 2018. He is currently the General Coordinator of the EU-Funded Innovative Training Network Project METAWIRELESS, on the application of metasurfaces to wireless communications, and the Doctoral Network ISLANDS, on the integrated sensing and communications for the vehicular environment. He has coauthored about 170 technical peer-reviewed journals and conference papers, and, among these, the highly cited paper "What will 5G be?," IEEE JOURNAL ON SELECTED AREAS IN COMMUNICATIONS, in June 2014. His current research interests include communications and signal processing, with an emphasis on wireless communications and beyond-5G systems.

Dr. Buzzi is a TPC member for several international conferences. He is a former Associate Editor of the IEEE SIGNAL PROCESSING LETTERS and the IEEE COMMUNICATIONS LETTERS and has been the Guest Editor of four IEEE JOURNAL ON SELECTED AREAS IN COMMUNICATIONS Special Issues. From 2014 to 2020, he has been an Editor of the IEEE TRANSACTIONS ON WIRELESS COMMUNICATIONS. Currently, he is an Associate Editor of the IEEE TRANSACTIONS ON COMMUNICATIONS.

Open Access funding provided by 'Università degli Studi di Cassino e del Lazio Meridionale' within the CRUI CARE Agreement